University of Reading

Evaluating the relationship between interannual variations in the Antarctic ozone hole and Southern Hemisphere surface climate in chemistry-climate models

Article

Accepted Version

Gillett, Z. E., Arblaster, J. M., Dittus, A. J. ORCID: https://orcid.org/0000-0001-9598-6869, Deushi, M., Jöckel, P., Kinnison, D. E., Morgenstern, O., Plummer, D. A., Revell, L. E., Rozanov, E., Schofield, R., Stenke, A., Stone, K. A. and Tilmes, S. (2019) Evaluating the relationship between interannual variations in the Antarctic ozone hole and Southern Hemisphere surface climate in chemistry-climate models. Journal of Climate, 32 (11). pp. 3131-3151. ISSN 0894-8755 doi: 10.1175/JCLI-D-18-0273.1 Available at https://centaur.reading.ac.uk/82669/

It is advisable to refer to the publisher's version if you intend to cite from the work. See Guidance on citing.

To link to this article DOI: http://dx.doi.org/10.1175/JCLI-D-18-0273.1

Publisher: AMS

University of Reading

All outputs in CentAUR are protected by Intellectual Property Rights law, including copyright law. Copyright and IPR is retained by the creators or other copyright holders. Terms and conditions for use of this material are defined in the End User Agreement.

www.reading.ac.uk/centaur

CentAUR

Central Archive at the University of Reading

Reading's research outputs online

Evaluating the relationship between interannual variations in the Antarctic Ozone Hole and Southern Hemisphere surface climate in chemistry-climate models

Zoe E. Gillett[1,2*], Julie M. Arblaster[1,2,3], Andrea J. Dittus[1,4], Makoto Deushi[5], Patrick Jöckel[6], Douglas E. Kinnison[3], Olaf Morgenstern[7], David A. Plummer[8], Laura E. Revell[9,10,11], Eugene Rozanov[9,12], Robyn Schofield[13,14], Andrea Stenke[9], Kane A. Stone[13,14,a], and Simone Tilmes[3]

[1]*School of Earth, Atmosphere and Environment, Monash University, Melbourne, Australia*

[2]*ARC Centre of Excellence for Climate Extremes, Australia*

[3]*National Center for Atmospheric Research, Boulder, USA*

[4]*NCAS-Climate, Department of Meteorology, University of Reading, UK*

[5]*Meteorological Research Institute, Tsukuba, Japan*

[6]*Deutsches Zentrum für Luft- und Raumfahrt, Institut für Physik der Atmosphäre, Oberpfaffenhofen, Germany*

[7]*National Institute of Water and Atmospheric Research, Wellington, New Zealand*

[8]*Climate Research Branch, Environment and Climate Change Canada, Montreal, Canada*

[9]*Institute for Atmospheric and Climate Science, ETH Zürich, Zürich, Switzerland*

[10]*Bodeker Scientific, Christchurch, New Zealand*

[11]*School of Physical and Chemical Sciences, University of Canterbury, Christchurch, New Zealand*

[12]*Physikalisch-Meteorologisches Observatorium Davos/World Radiation Center, Davos, Switzerland*

[13]*School of Earth Sciences, University of Melbourne, Melbourne, Australia*

[14]*ARC Centre of Excellence for Climate System Science, Australia*

[a]*now at: Massachusetts Institute of Technology, Cambridge, Massachusetts, USA*

**Corresponding author address:* Zoe E. Gillett, School of Earth, Atmosphere and Environment, 9 Rainforest Walk, Monash University, VIC 3800, Australia

E-mail: zoe.gillett@monash.edu

ABSTRACT

Studies have recently reported statistically significant relationships between observed year-to-year spring Antarctic ozone variability and the Southern Hemisphere Annular Mode and surface temperatures in spring-summer. This study investigates whether current chemistry-climate models (CCMs) can capture these relationships, in particular, the connection between November total column ozone (TCO) and Australian summer surface temperatures, where years with anomalously high TCO over the Antarctic polar cap tend to be followed by warmer summers. The interannual ozone-temperature teleconnection is examined over the historical period in the observations and simulations from the Whole Atmosphere Community Climate Model (WACCM) and nine other models participating in the Chemistry-Climate Model Initiative (CCMI). There is a systematic difference between the WACCM experiments forced with prescribed observed sea surface temperatures (SSTs) and those with an interactive ocean. Strong correlations between TCO and Australian temperatures are only obtained for the uncoupled experiment, suggesting that the SSTs could be important for driving both variations in Australian temperatures and the ozone hole, with no causal link between the two. Other CCMI models also tend to capture this relationship with more fidelity when driven by observed SSTs, though additional research and targeted modelling experiments are required to determine causality and further explore the role of model biases and observational uncertainty. The results indicate that CCMs can reproduce the relationship between spring ozone and summer Australian climate reported in observational studies, suggesting that incorporating ozone variability could improve seasonal predictions, however more work is required to understand the difference between the coupled and uncoupled simulations.

1. Introduction

The Antarctic ozone hole has formed each austral spring since the early 1980s where up to half of the total column ozone (TCO) is depleted (Solomon 1999; World Meteorological Organization (WMO) 2014). Though it has little impact on global temperatures, this long-term ozone depletion has likely influenced the Southern Hemisphere (SH) atmospheric circulation and thus the surface climate. It cools the SH polar stratosphere and strengthens the polar vortex; and is associated with a summertime poleward shift and strengthening of the midlatitude jet (Lee and Feldstein 2013; Seviour et al. 2017), strongly associated with the positive phase of the Southern Annular Mode (SAM), the leading mode of climate variability in the SH extratropical circulation (Trenberth 1979; Rogers and van Loon 1982). While increasing greenhouse gases (GHGs) also force a positive summer SAM trend (e.g., Arblaster and Meehl 2006; McLandress et al. 2011; Grise and Polvani 2017), model experiments that have compared the influence of both factors individually have suggested that ozone depletion is likely the dominant factor (e.g., Arblaster and Meehl 2006; McLandress et al. 2011; Polvani et al. 2011; Stone et al. 2016).

In addition to the long-term trend, the size of the ozone hole varies substantially between years due to dynamical processes (Salby et al. 2011, 2012). Years with anomalously small ozone holes are usually associated with stronger winter planetary wave forcing that transports more ozone to the polar region and warms the Antarctic stratosphere, thus weakening the polar vortex. The warmer temperatures inhibit the formation of polar stratospheric clouds that deplete ozone via chemical reactions and hence reduce ozone loss (Salby et al. 2011, 2012). This year-to-year variability in the size of the ozone hole has been linked to variability in the SAM and surface temperatures in the SH. Son et al. (2013) reported a statistically significant negative correlation between September ozone concentration and the October SAM index. Bandoro et al. (2014) further reported a significant relationship between November TCO and seasonal mean summer surface temperatures in the SH midlatitudes, including Australia; with unusually

99 hot summers associated with anomalously small ozone holes (higher TCO) in the previous
100 spring. The connection between spring ozone and summer temperature over Australia is thought
101 to arise due to the link between ozone and the SAM. A negative SAM in summer (associated
102 with high spring ozone) causes anomalous westerly surface winds that lead to decreased
103 precipitation and warmer surface temperatures over subtropical eastern Australia in summer
104 (Hendon et al. 2007; Son et al. 2013; Bandoro et al. 2014).

105 Australian summer temperature extremes are influenced by large-scale modes of
106 climate variability including the El Niño-Southern Oscillation (ENSO), Indian Ocean Dipole
107 and SAM (Hendon et al. 2007; Risbey et al. 2009; Arblaster and Alexander 2012; Min et al.
108 2013). ENSO has some predictability on seasonal time scales and has, therefore, traditionally
109 been the main component considered in operational seasonal forecasts (McBride and Nicholls
110 1983) before the implementation of a dynamical seasonal forecast system (Hudson et al. 2016).
111 The observed connection between spring Antarctic ozone and Southern Hemisphere climate
112 suggests that including real-time stratospheric ozone variability could potentially improve skill
113 in seasonal outlook systems. This is particularly timely as extreme summers in Australia are
114 likely to become more common under future emission scenarios (e.g., Perkins et al. 2015;
115 Perkins-Kirkpatrick et al. 2016). Improved seasonal forecasting could, therefore, be an
116 important adaptation tool for mitigating the impacts of extreme heat events.

117 However, climate models must be able to reliably simulate ozone behaviour and
118 stratospheric-tropospheric dynamics to produce accurate forecasts. Chemistry-Climate Models
119 (CCMs) are perhaps the most useful model to address these interactions as chemistry is fully
120 interactive and coupled to dynamics and radiation; and CCMs, therefore, tend to simulate the
121 impacts of ozone on the circulation and climate better than models with prescribed ozone (e.g.,
122 Son et al. 2008; Li et al. 2016). Since chemical reactions cause the ozone hole, it is critical that

123 interactive chemistry is included in the model to capture and predict these interannual
124 relationships.

125 Many climate model studies have examined the long-term impact of Antarctic ozone
126 depletion on stratospheric and tropospheric circulation and climate (e.g., Gillett and Thompson
127 2003; McLandress et al. 2011; Polvani et al. 2011) but few have addressed the impact on
128 interannual timescales. Fogt et al. (2009) and Li et al. (2010) reported that a CCM captures
129 observed interannual ozone-SAM and SAM-Brewer-Dobson circulation relationships,
130 respectively. However, a deficiency common to these models is related to a "cold pole" bias
131 present in many CCMs (Eyring et al. 2006) which further delays the breakdown of the polar
132 vortex and likely causes the model to overpredict the impacts of the ozone hole (Lin et al. 2017).
133 Moreover, Seviour et al. (2014) reported that the October mean SAM could be forecast from
134 midstratospheric anomalies at the beginning of August, and Dennison et al. (2015) showed that
135 during the period of ozone depletion, the tropospheric circulation is influenced for up to two
136 months following a stratospheric SAM extreme event. To date, there has yet to be a study that
137 has examined whether climate models can simulate the interannual link between ozone and
138 surface temperatures; and hence, the possibility of improving seasonal forecasts.

139 The purpose of the present study is to investigate the potential for predicting summer
140 surface temperature extremes using ozone variability. This involves examining historical
141 simulations from the Whole Atmosphere Community Climate Model (WACCM) and other
142 CCMs to assess whether these models can capture the influence of the interannual variability
143 in the Antarctic spring ozone hole on summer temperatures, with a focus over the Australian
144 continent. This is a necessary first step in examining the potential for its inclusion in a seasonal
145 prediction system.
146

2. Data and analysis method

a. Observational and reanalysis data

Multiple observational datasets for TCO and surface temperature are used in this study to examine sensitivity to observation and reanalysis uncertainty. Monthly mean TCO fields have been obtained from the NIWA-BS (National Institute of Water and Atmospheric Research – Bodeker Scientific) database (Bodeker et al. 2005; http://www.bodekerscientific.com/data/total-column-ozone). The NIWA-BS data averaged over the polar cap (63-90°S), are mainly compared to TCO from the Halley Station (herein Halley) which measures ozone variability at a single grid point (75°S, 26°W; https://legacy.bas.ac.uk/met/jds/ozone/data/ZOZ5699.DAT). TCO from the South Pole (90°S, 25°W) and Syowa (69°S, 39°E) stations (http://www.woudc.org) are also examined. Monthly mean surface temperatures are obtained from the Interim reanalysis of the European Centre for Medium-Range Weather Forecasts (ERA-Interim; Dee et al. 2011). ERA-Interim is compared to monthly surface temperature from the Australian Water Availability Project (AWAP; Jones et al. 2009) which is a gridded dataset based on station data. Monthly mean maximum and minimum temperatures for AWAP were averaged to produce monthly mean temperature. The Marshall (2003) SAM index (http://www.nerc-bas.ac.uk/public/icd/gjma/newsam.1957.2007.txt) and ENSO are used to examine links between ozone and modes of climate variability. Gridded observed monthly SSTs from the Hadley Centre Ice and Sea Surface Temperature dataset (Rayner et al. 2003) were used to calculate the Niño 3.4 index (described in Section 2d).

b. Model output

This study uses the output from version 1 of WACCM, conducted as part of the Chemistry-Climate Model Initiative (CCMI; Eyring et al. 2013). WACCM is a fully interactive

CCM where chemistry is coupled with dynamics and radiation, and this, therefore, permits chemistry-climate feedbacks. WACCM was chosen as the primary model analysed as it has been shown to have excellent agreement with observations in the evolution of the Antarctic ozone hole (Marsh et al. 2013) and is one of a limited number of CCMs that is coupled to an ocean (Morgenstern et al. 2017), which is an important characteristic for seasonal prediction. The model domain extends from the surface to 140 km with 66 hybrid sigma-pressure levels, and horizontal resolution of 1.9° latitude by 2.5° longitude (Marsh et al. 2013).

Four WACCM experiments are analysed in this study to examine the role of ocean coupling for stratospheric-tropospheric relationships and the influence of ozone-depleting substances (ODSs) and GHGs individually. Each experiment has an ensemble of three or five transient simulations that have slightly different initial conditions (Eyring et al. 2013; Morgenstern et al. 2017) and cover 1960-2005:

- REF-C1 (or uncoupled): uses an atmosphere-only model configuration forced with observed SSTs and sea ice and historical radiative forcings (GHGs, ODSs, tropospheric ozone and aerosols, quasi-biennial oscillation, very short-lived species, volcanic aerosols, and solar variability)
- REF-C2 (or coupled): uses the identical atmospheric configuration and historical radiative forcings as REF-C1 but is fully coupled to an interactive ocean and sea ice component, and extends to 2100 following the A1 scenario for ODSs (WMO 2014) and Representative Concentration Pathway 6.0 scenario (Meinshausen et al. 2011)
- SEN-C2-fODS1960 (herein ODS1960): the same as REF-C2 but with ODSs containing chlorine and bromine set at 1960 levels. Thus, interannual variations in the size of the Antarctic ozone hole will still occur due to dynamic variability, but no ozone depletion is simulated

- SEN-C2-fGHG (herein GHG1960): the same as REF-C2 but with anthropogenic GHGs fixed at 1960 levels.

The WACCM uncoupled experiment has five simulations available; and unless stated otherwise, for consistency, only the first three were used to avoid a larger sample size biasing the results compared to the coupled model ensemble. The other two members were tested and produce quantitatively similar results to the three members used in this study.

To examine the strength of the findings in WACCM and evaluate the impact of model biases, nine other CCMI models are included (ACCESS-CCM, CESM1 CAM4-Chem, CMAM, EMAC-L47MA, EMAC-L90MA, GEOSCCM, MRI-ESM, NIWA-UKCA, and SOCOL; model specifics are available in Morgenstern et al. (2017)). In total, this facilitates analysis of five models with a coupled ocean for REF-C2 and five with an uncoupled ocean that prescribe SSTs and sea ice concentrations using simulations from another climate model. For the CCMs without an ocean, different SSTs and sea ice concentrations were used for REF-C1 and REF-C2. All ensemble members available on the British Atmospheric Data Center were included. For the additional models, the lowest model level was used for the temperature at the surface. We compared the difference between the surface temperature field and lowest model level in the correlation analysis for WACCM, and the difference was negligible.

c. Analysis period

This study examines the period 1979-2005, which represents the overlap period for the satellite data and the model historical period. These years are selected as studies have reported that the relationship between interannual variations in Antarctic ozone and SH surface climate is strengthened during the period of ozone depletion (Fogt et al. 2009; Bandoro et al. 2014) as the ozone hole delays the polar vortex breakdown and leads to increased coupling between the stratosphere and troposphere (Shaw et al. 2011). The Antarctic ozone layer has also shown

signs of recovery since 2000 (e.g., Solomon et al. 2016; Chipperfield et al. 2017), and the years before this were, therefore, when stratospheric ozone depletion was largest overall. November ozone and summer (December-January-February) surface temperatures are the focus of this study for comparison with Bandoro et al. (2014) and when temperature extremes arguably cause more impact. Ozone variability throughout the year in WACCM is in good agreement with observations and tends to peak in October-November, similar to observations (Table A1; Roff et al. 2011; Son et al. 2013; Bandoro et al. 2014). Apart from Section 3e, all model analysis is conducted for WACCM.

d. Indices

The ozone hole is defined as the weighted area average TCO over the polar cap (63-90°S), after similar studies (e.g., Son et al. 2013). The ozone index is calculated for September to April only, as observations are unavailable in other months due to polar night. Figure 1a and b show the time series of the ozone index in November for the first member of the WACCM uncoupled and coupled experiments, respectively. The interannual variability of the ozone hole and all indices are obtained by first removing the long-term linear trend (Fig. 1c and d), following Bandoro et al. (2014). Detrending the data also removes the linear influence of GHG increases.

For WACCM, the SAM index is defined as the difference in standardised zonal mean sea level pressure (SLP) between 40°S and 65°S, following Gong and Wang (1999). Strong SAM events are identified when the value is greater or less than one standard deviation (after detrending). The Niño 3.4 index (5°S-5°N and 170-120°W; Trenberth 1997), is used to analyse the ENSO influence on ozone and SAM.

246 *e. Correlations and composites*

247 Pearson correlation coefficients were calculated between ozone and other variables,
248 after first removing the annual cycle and detrending. These links are examined throughout the
249 year using lag correlations, with the ozone index correlated to each 3-month overlapping
250 surface temperature or SAM period for up to 6 months. To explore the relationships further
251 over Australia, we focus on area-averaged surface temperature in Eastern Australia (10-44°S
252 and 141-156°E; where at least 50% of each grid box had to be comprised of land surface to be
253 included in the calculation) as Bandoro et al. (2014) found that the relationship between
254 November ozone and summer surface temperatures was largest in this region. For analysis with
255 WACCM, the three 26-year timeseries from each experiment were concatenated (unless stated
256 otherwise) to provide a larger sample than is possible with the observations and improve the
257 signal-to-noise ratio.

258 To investigate the influence of large ozone (SAM) anomalies on stratospheric and
259 tropospheric climate, years with high and low November ozone (summer SAM) were identified
260 as years that exceed one standard deviation (after first removing the annual cycle, detrending
261 and concatenating the three members) (Fig. 1c and d). Composites were then created for the
262 difference between years with high and low November ozone (summer SAM). Statistical
263 significance of correlations and composites were assessed using a two-sided Student *t* test with
264 the degrees of freedom reduced based on the lag-1 autocorrelation, following Bretherton et al.
265 (1999) and Santer et al. (2000).

266

267 **3. Results**

268 *a. Ozone-SAM relationship*

269 The main interest of this paper is the interannual impact of the Antarctic ozone hole on
270 surface temperatures. As the impacts of ozone depletion on surface climate resemble the SAM

(see, e.g., Thompson et al. 2011), the interannual link between ozone and SAM is first explored. Figure 2 shows lag correlations between ozone and SAM (the time reference is based on the ozone index) for Halley ozone (75°S, 25°W, Fig. 2a), NIWA-BS ozone (averaged 63-90°S, Fig. 2b) and the four WACCM experiments (averaged 63-90°S, Fig. 2c-f) where the three ensemble members for each experiment were first concatenated.

The observations and WACCM experiments all capture strong negative correlations between spring ozone and SAM in the following months, implying that smaller (larger) spring ozone holes are associated with decreases (increases) in the SAM. This association is consistent with long-term ozone depletion leading to a more positive SAM in summer (Thompson et al. 2011). Though, it is unclear if interannual ozone variations drive variations in the SAM through the same mechanism by which stratospheric ozone depletion influences the SAM, as other factors, such as winter-spring wave driving, also influence SAM and ozone variations (Thompson et al. 2005; Son et al. 2013; Seviour et al. 2014) and it is difficult to separate cause and effect. Note that while we are focussed on the use of ozone for prediction, Fogt et al. (2009) previously found significant negative correlations between observed ozone and SAM also at negative lags, indicating that when the SAM is weak, more ozone is transported to the polar vortex.

There are substantial differences between observational datasets and between model experiments. In the observations, correlations are largest for September-October ozone, whereas the WACCM experiments peak one month later in November-December. A possible cause for the delayed onset in the model experiments could be due to the cold pole bias. For example, Sheshadri and Plumb (2016) found in an idealised atmosphere model that the surface response to polar stratospheric cooling (indicative of ozone depletion) is sensitive to the timing of the cooling. The ozone-SAM link is weaker and less persistent for Halley (Fig. 2a) and could be a consequence of this station being located at the edge of the polar vortex in some parts of

296 the year. Both observational datasets and the WACCM coupled and uncoupled experiments
297 capture a band of positive correlations in March-April; which have been linked to natural
298 variability in the polar vortex (Fogt et al. 2009; Smith and Polvani 2017). Furthermore, the
299 SAM response to ozone concentrations seems to be too persistent in the WACCM coupled
300 experiment (Fig. 2d) compared to the atmosphere-only configuration (Fig. 2c), especially in
301 summer.

302 The differences between the sensitivity and all forcing experiments provide some
303 indications of the forcings driving observed ozone-SAM links. The GHG1960 experiment (Fig.
304 2e) looks like the all forcing (coupled) experiment, indicating that ozone depletion is the main
305 driver of this interannual relationship. There are still significant correlations when ODSs are
306 fixed at 1960 levels (Fig. 2f), although the correlations are less persistent, suggesting that long-
307 term ozone depletion has increased the strength of the ozone-SAM relationship, as also found
308 by Fogt et al. (2009).

309

310 *b. Ozone-temperature relationship*

311 Figure 3 is similar to Fig. 2; however, it shows lag correlations between ozone and
312 Eastern Australia surface temperature. Eastern Australia was chosen for the reference region as
313 the observational study by Bandoro et al. (2014) showed that the correlation between November
314 ozone and summer surface temperatures was largest in this region. The observations capture
315 significant positive correlations between spring ozone months and seasonal Eastern Australia
316 surface temperature; where years with smaller (larger) ozone holes are typically associated with
317 warmer (cooler) temperatures in spring and summer (Fig. 3a-d). Though, as mentioned earlier,
318 this result does not demonstrate causality. It is difficult to separate the roles of the polar vortex,
319 wave-driving and ozone concentrations as they are closely related, however substituting 10 hPa
320 geopotential heights averaged over the polar cap for ozone leads to weaker correlations with

Australian temperature in the model. In complementary results to ours, a recent study by Lim et al. (2018) showed an index of the SH polar vortex is correlated with October and November ozone and with Australian October-January surface temperature.

There are differences between observational datasets, especially when using Halley ozone (Fig. 3a and b), and correlations are less significant overall for AWAP and Halley, compared to ERA-Interim and Halley. A distinct separate band of significant positive correlations is seen for the Halley and ERA-Interim correlations for February ozone (Fig. 3a), which is absent in the other observational correlations. These positive correlations are largest in autumn ($p < 0.01$) and could be related to a trend toward the positive SAM in April-May (Thompson and Solomon 2002; Ivy et al. 2017). As this second band of significant positive correlations is missing for the other datasets, this suggests that there is some uncertainty in the ozone-Australian surface temperature relationship.

It is in the link between ozone and surface temperature that noticeable differences between the WACCM experiments begin to appear. The uncoupled experiment captures significant correlations between spring ozone and Eastern Australian surface temperature in the subsequent seasons (Fig. 3e), broadly like the observations, although it peaks slightly later and has significant positive correlations during more months of the year and for longer lags than observed. Studies have found that CCMs tend to overpredict interannual stratosphere-troposphere relationships due to the polar vortex breaking down later than observed (Fogt et al. 2009; Li et al. 2010). This bias may contribute to the overestimated response in the uncoupled experiment (see also Section 3a) and likely has implications for improved seasonal forecasting using ozone. Unlike the uncoupled experiment and observations, the coupled experiment does not capture a significant relationship between spring ozone and spring-summer temperatures (Fig. 3f).

345 The WACCM sensitivity experiments again provide some insight as to the forcings
346 contributing most to the ozone and Australian temperature teleconnection. In the GHG1960
347 experiment (Fig. 3g), there are strong, positive correlations between the year-to-year size of the
348 ozone hole and Eastern Australia surface temperature. These correlations are largest in
349 November but occur for more months in the year than observed, like the uncoupled experiment
350 (Fig. 3e). In the ODS1960 experiment (Fig. 3h), there are weak and insignificant correlations
351 between ozone and surface temperature for most months in the year, similar to the coupled
352 experiment. Thus, the impact of GHGs alone results in a weaker response, consistent with
353 previous results (e.g., Fogt et al. 2009; Bandoro et al. 2014) that suggest that long-term ozone
354 depletion has led to an increase in interannual ozone variability (Table A1) and is, therefore,
355 more able to produce a signal that can influence the surface. The GHG1960 experiment uses
356 the identical configuration to the coupled experiment but with GHGs fixed at 1960 levels. This
357 experiment captures significant correlations between ozone and Eastern Australia surface
358 temperature (Fig. 3g) unlike the all-forcing experiment (Fig. 3f) indicating that the WACCM
359 coupled model can simulate this observed connection, but time-evolving GHGs appear to
360 weaken the relationship. We speculate that this could be related to the interactive impact of
361 increasing GHGs on sea ice and SSTs in this model. For example, similarly to most coupled
362 climate models, Antarctic sea ice extent undergoes large declines over the historical period in
363 the coupled experiment, in contrast to the observed increase over the satellite era (Marsh et al.
364 2013). This decline would likely impact interannual variability in the SAM (e.g., Kidston et al.
365 2011; Raphael et al. 2011) and hence Australian surface temperatures, although this hypothesis
366 requires further investigation with additional models.
367 To provide a global view, surface temperature from ERA-Interim is used for all
368 observational analysis conducted herein. Figure 4 shows the spatial pattern of correlation
369 coefficients of November ozone and summer surface temperatures. These months are examined

370 in detail to evaluate whether WACCM can capture the observed link between November ozone
371 and summer temperatures over Australia found by Bandoro et al. (2014). The two observational
372 ozone datasets (Halley and NIWA-BS) have very similar regional structures (Fig. 4a and b),
373 despite differences in the ozone hole definition and data collection method, indicating that the
374 large-scale patterns are mostly unaffected by these factors. In the Australian region, correlations
375 are largest over southern and eastern Australia. The observed correlations for the period 1979-
376 2004 are not statistically significant over Australia like in the 1979-2012 period (not shown)
377 used by Bandoro et al. (2014), but the pattern is similar.

378 The WACCM experiments (Fig. 4c and d) capture similar relationships to the
379 observations over the Antarctica polar cap, regarding sign and magnitude, however, away from
380 this region, there are noticeable differences in the spatial pattern. The uncoupled experiment
381 has more significant correlations in the tropical Pacific and Indian Oceans and tends to simulate
382 stronger correlations overall than observed (Fig. 4c). Notably, both model experiments
383 incorrectly simulate the sign of the correlations over the Indian Ocean and have weaker
384 magnitude over the Southern Ocean. The uncoupled experiment captures strong positive and
385 significant correlations over Australia, with the largest correlations in the south-southeast,
386 consistent with the observations; whereas, the coupled experiment only has low correlations
387 over Australia, as expected from Fig. 3f.

388 Figure 5 displays the correlation coefficients between November ozone and summer
389 surface temperature in Eastern Australia. For the observations, we compared correlations
390 calculated using Halley and NIWA-BS ozone with TCO from Syowa and South Pole stations
391 (Fig. 5). The relationship is weaker using South Pole ozone and strongest using Syowa ozone
392 instead of Halley ozone, consistent with van Ommen and Morgan (2010) who found a
393 significant relationship between Antarctic snowfall in the Indian Ocean sector and southwest
394 Australian rainfall. The correlations between November ozone and Eastern Australia summer

surface temperature in the WACCM coupled experiment are weaker overall than the uncoupled experiment and observations (Fig. 5). Using the correlation coefficients for each ensemble member of the WACCM coupled and uncoupled experiments, we conducted an unpaired two-sample t-test to assess the significance of the difference of the means. This analysis shows that the difference in the correlation coefficients between the WACCM uncoupled and coupled experiments is statistically significant at the 5% level.

Figure 5 also shows correlations for the ensemble mean of the WACCM uncoupled and coupled experiments. The ensemble mean reduces the natural variability through averaging and thus helps to isolate the forced response. The ensemble mean correlation is larger than the original correlation in both WACCM experiments, indicating that the forcings (i.e., the historical forcings as well as the SSTs and sea ice in the uncoupled experiment) are enhancing the interannual signal. Given the time series are detrended, it indicates that either some portion of the GHG or ODS forced changes have not been removed through linear regression or that additional forcings are contributing to the interannual relationships found.

Given the ensemble mean of the uncoupled experiment has larger correlations than the individual ensemble members (Fig. 5), this suggests that part of the ozone-temperature relationship is due to the boundary conditions (SSTs and sea ice) driving both interannual variations in ozone and variations in Australian temperature. To test this hypothesis, we subtracted the ensemble mean ozone and Australian temperature from each ensemble member and repeated the calculation with the concatenated ensemble members. This removes the response to the historical forcings and driving SSTs, and the resulting anomalies represent the response to internally generated ozone variations. The correlations were reduced to a similar magnitude as the coupled experiment (Table 1), therefore confirming our hypothesis.

It is somewhat surprising that the ensemble mean correlation is also enhanced in the coupled model experiment (Fig. 5) since the influence of SSTs will be removed through

420 averaging. Given the timeseries are detrended, this points to the role of a non-linear external
421 forcing. Large volcanic eruptions have been shown to impact global mean temperature and
422 significantly deplete stratospheric ozone over Antarctica (e.g., McCormick et al. 1995;
423 Solomon et al. 2016; Stone et al. 2017). When the years corresponding to the El Chichón (1982)
424 and Mount Pinatubo (1991) eruptions were removed from the temperature and ozone time series
425 and the ensemble mean was recalculated, in the WACCM coupled experiment, the ensemble
426 mean correlations are substantially reduced (Table 1). This suggests that the impact of these
427 eruptions on the ozone hole and Australian temperatures is reinforced in the ensemble mean
428 and the ozone hole and Australian temperatures are responding to the volcanic forcings. Most
429 of the signal in the uncoupled experiment appears to be coming from the SSTs as the ensemble
430 mean correlations only show minor decreases when the major volcanic eruptions are removed
431 (Table 1).

432 The WACCM uncoupled experiment appears to have a very strong ENSO response
433 (Fig. 4c), and the summer Niño 3.4 index is significantly correlated with November ozone
434 unlike in the observations or coupled experiment (Table 2). However, strong correlations are
435 still obtained after the ENSO signal is removed from surface temperatures (Table 1), via linear
436 regression against the summer Niño 3.4 index, consistent with the observational study of
437 Bandoro et al. (2014). In the coupled experiment, the relationship between ozone and
438 temperature is strengthened after ENSO is removed from surface temperatures (Table 1).

439

440 *c. Analysing differences between model experiments*

441 Section 3b demonstrated that a CCM (WACCM) could capture the ozone-temperature
442 teleconnection over Australia, including the observed link between November ozone and
443 summer surface temperature. However, this is not the case for the WACCM coupled
444 experiment, as it only captures weak correlations that are not significant (Figs. 4d and 5). The

445 analysis conducted in Section 3c and d, therefore, focuses on understanding why the WACCM
446 coupled experiment cannot capture the observed relationship.

447 To assess the differences between the WACCM uncoupled and coupled experiments,
448 composites are now used; taking the differences between years with high and low November
449 ozone, defined as years greater than one standard deviation. Figure 6 shows the vertical profile
450 of polar cap geopotential height as a function of month. Higher geopotential heights are
451 observed over Antarctica in years with high ozone (Fig. 6), consistent with the negative phase
452 of the SAM. The difference between the two experiments is largest in the troposphere rather
453 than the stratosphere (tropopause located at approximately 200 hPa over Antarctica). In the
454 uncoupled experiment, stratospheric anomalies appear to be followed by similar signed
455 anomalies in the troposphere, shown by the significant differences between high-low years, and
456 these anomalies reach the surface in late spring to early summer (Fig. 6a). These tropospheric
457 composite differences in December-January are consistent with observations (Thompson and
458 Solomon 2002) where surface anomalies lag stratospheric anomalies by one season, but appear
459 to reach the surface too early in late spring. In the WACCM coupled experiment, there is also
460 downward migration in summer (Fig. 6b); however, it is weaker and not significant. Less
461 downward influence in the coupled experiment could also be related to the somewhat weaker
462 interannual variability in the SAM (Table A2).

463 Despite the differences shown in Fig. 6, the coupled experiment can simulate the link
464 between ozone and the SAM (Fig. 2d and Table 3). Thus, the relationship between ozone and
465 surface temperatures appears to break down in the link between the circulation and
466 temperatures, rather than in the link between ozone and the circulation.

467 Figure 7 shows the difference in the tropospheric and surface response in summer
468 between years with high and low November ozone in the observations. The responses are
469 similar between the Halley and NIWA-BS ozone datasets and ozone hole indices but are weaker

overall for NIWA-BS. Years with high ozone are associated with easterly wind anomalies over Australian latitudes (Fig. 7c and d), and warmer temperatures across southern-southeastern Australia (Fig. 7a and b), and the SLP field resembles the negative phase of the SAM (Fig. 7e and f).

Figure 8 is like Fig. 7 but for the WACCM uncoupled and coupled experiments. In the uncoupled experiment, years with high November ozone are associated with significant warm anomalies of up to 2 degrees over Australia and a warming of the equatorial Pacific Ocean in summer (Fig. 8a). A strong signal can be seen over the Southern Ocean in the 500 hPa zonal wind in the uncoupled experiment (Fig. 8c), corresponding to an equatorward shift and change in the strength of the 500 hPa midlatitude jet during high ozone years or the negative SAM. In comparison, the coupled experiment does not produce a clear surface temperature difference between high and low ozone years and does not exhibit an ENSO signature (Fig. 8b).

The contrast between the observations and WACCM and the difference between the WACCM uncoupled and coupled experiments is largest in the SLP field (Figs. 7e and f and 8e and f). In the uncoupled experiment, there is a Pacific South American (PSA) wave train (Karoly 1989). The SAM has been shown to strongly resemble the PSA pattern in the Pacific (Ding et al. 2012) and the PSA is related to ENSO on interannual timescales (Mo 2000), indicating that variability in SSTs in the equatorial central-eastern Pacific is linked to the SAM (i.e., ozone) and may strengthen the link between ozone and Australian temperatures. The uncoupled experiment still produces strong correlations between ozone and Australian temperatures when the ENSO signal is removed (Table 1), despite looking like a typical El Niño response (Fig. 8a and e; Zubiaurre and Calvo 2012), indicating that ozone variability can sufficiently induce changes in the SAM and impact surface temperatures. In contrast, the coupled experiment looks more like zonal wave number 3 (Fig. 8f; Raphael 2004) which alters the wind patterns and temperature response over Australia. Unlike observed (Fig. 7e and f), the

SAM signal is less distinct in WACCM (Fig. 8e and f). Though, the PSA/ENSO and zonal wave number 3 patterns are linked to the SAM: ENSO and SAM are strongly correlated in the late spring and early summer (e.g., L'Heureux and Thompson 2006; Lim et al. 2013) and the amplitude of wave number 3 is related to the phase of SAM (Turner et al. 2017). The different responses between the uncoupled and coupled experiments could also be related to the ENSO response to ozone being too strong in the uncoupled case (Table 2).

d. Model biases

A coupled ocean in WACCM appears to change the atmospheric and surface response to interannual ozone variability. The coupled experiment may not capture the observed ozone-Australian temperatures teleconnection because the evolution of observed SSTs may be crucial to the relationship. Given the ensemble mean of the uncoupled experiment shows a higher correlation coefficient, we suggest that the SSTs could be driving both interannual variations in ozone and Australian temperatures, although, it is likely that the overall ability of a model to reproduce this relationship is also influenced by model biases.

Figure 9 shows the observed and simulated correlations for Eastern Australia summer surface temperatures with SSTs and SLP, respectively. Australian summer surface temperatures are influenced by ENSO, SAM and the Indian Ocean (Fig. 9a and b). The WACCM uncoupled experiment broadly captures these correlations (Fig. 9c and d) in all basins. In the coupled experiment, however, Eastern Australia summer temperatures are dominated by strong anomalies in the tropical Pacific and Indian Oceans (Fig. 9e and f). These tropical model biases may be overwhelming the SAM response and inhibiting the interannual link between ozone and Eastern Australian surface temperatures via the SAM. This is supported by the fact that removing the ENSO signal from surface temperatures in the WACCM coupled experiment (Table 1) slightly increases the strength of the relationship between November ozone and

summer surface temperature in Eastern Australia. Model biases in the Indian Ocean (e.g., Lim and Hendon 2015) may also result in interference in the surface response in the coupled case.

Table 4 shows the correlation coefficients between summer ENSO and SAM with Eastern Australia summer surface temperature. In the WACCM uncoupled experiment, ENSO explains up to 22% ($p < 0.01$) of the interannual variability in Australian temperatures, which is close to the observations where ENSO explains 20% ($p < 0.1$). However, the influence of ENSO in the coupled experiment is too strong and explains more than 50% ($p < 0.01$, Table 4). The difference between the uncoupled and coupled experiments is highlighted particularly in the impact of SAM on Australian temperatures. While both experiments capture a strong and significant relationship between ozone and SAM (Fig. 2c and d and Table 3), the coupled model poorly simulates the connections between ozone and SAM with Australian temperatures (Figs. 3f, 4d and 5 and Table 4). Similar results for the low-top version of the WACCM model (CCSM4; Table 4) indicate that this bias is not related to the inclusion of interactive chemistry or a more resolved stratosphere in WACCM but a likely breakdown in tropical-extratropical interactions in this version of the atmosphere, potentially related to the overestimated magnitude of ENSO (Deser et al. 2012; Marsh et al. 2013). The most recent version of the low-top model (CESM1-CAM5) has a much-improved relationship between SAM and Australian temperatures (Table 4).

The different SAM responses between the WACCM uncoupled and coupled experiments are further highlighted in Fig. 10, the composite differences in summer between years in the high and low phases of the summer SAM. Over Australia, the positive phase of SAM is associated with cooler temperatures (Fig. 10a) related to the poleward shift of the midlatitude jet (Fig. 10d). The WACCM uncoupled experiment broadly resembles the observations, though with stronger temperature differences over Australia (Fig. 10b). In the coupled experiment, SAM does not appear to make a strong contribution to Australian

545 temperatures, shown by the weak temperature differences between high and low SAM (Fig.
546 10c). The composite temperature differences for the SAM for the coupled experiment also
547 appear to have an ENSO signature (Fig. 10c). Although this warming in the equatorial Pacific
548 Ocean is not significant, it is not seen in the observations or WACCM uncoupled experiment
549 and indicates that ENSO has a strong influence on the SAM during summer in this model
550 experiment. The coupled model SLP composites (Fig. 10i) also indicate positive anomalies in
551 the tropical Indian Ocean and western Pacific Ocean that are not observed and likely interfere
552 with the response to SAM over Australia.
553
554 *e. Additional models*
555 Figure 5 also shows the correlation coefficients between November ozone and summer
556 surface temperature in Eastern Australia for the nine additional CCMI models. These models
557 are organised in three groups: CCMI REF-C1, CCMI REF-C2-uncoupled (SSTs and sea ice
558 prescribed from another climate model), and CCMI REF-C2-coupled. Overall, most models
559 capture the correct sign for the correlation between November ozone and summer surface
560 temperatures in Eastern Australia, but there is large intermodel variability in the strength of the
561 correlation coefficients. Unlike in WACCM, there does not appear to be a systematic difference
562 between REF-C1 (uncoupled) and REF-C2 (coupled) for the other models. This suggests that
563 the SSTs might not be primarily driving the response, although they may contribute in part, but
564 rather that model biases are likely impacting most models' ability to reproduce the observed
565 interannual relationship between ozone and Australian summer surface temperature.
566
567 **4. Discussion**
568 This paper is the first to investigate the possibility of predicting seasonal temperatures
569 in Australia with ozone using a climate model. We have demonstrated that a climate model
570 with interactive chemistry can capture observed connections between interannual variability in

571 Antarctic TCO and Australian temperatures. Although CCMs are computationally expensive,
572 traditional models that prescribe an ozone climatology can severely underestimate the effects
573 of the ozone hole on climate (Li et al. 2016) and will not be able to capture this interannual
574 relationship.
575
576 *a. Interpretations of discrepancies between observations and models*
577 Section 3 demonstrated that the WACCM REF-C1 (observed SSTs and sea ice) and
578 REF-C2 (coupled ocean) experiments are both able to capture the interannual relationship
579 between ozone and SAM. However, the coupled experiment cannot simulate the interannual
580 relationships between ozone and Australian temperatures and SAM and Australian
581 temperatures, indicating that the relationship breaks down at the surface. Based on the analysis
582 conducted as part of this study, there are currently three plausible interpretations:
583 (1) That a strong relationship is only seen when the model is forced with observed
584 SSTs suggests that much of the observed signal could be due to the SSTs rather
585 than the Antarctic ozone hole, and the Australian temperatures and ozone hole
586 are simultaneously responding to the SSTs
587 (2) Model biases might hinder the ability of some climate models to simulate this
588 interannual relationship reliably
589 (3) Uncertainty in the observations could indicate that the connection between
590 ozone and Australian surface temperatures is not robust and could also be
591 influenced by natural decadal variability.
592 The first possibility is based on the results from WACCM where the observed SSTs and
593 sea ice appear to have an important role in the ozone and Australian temperatures relationship.
594 The results from the WACCM uncoupled experiment are consistent across all ensemble
595 members and increase for the ensemble mean, suggesting that SSTs could be driving variability

596 in both Australian temperatures and the ozone hole. This hypothesis is supported by the results
597 from REF-C2, where the coupled ocean and freely evolving SSTs and sea ice result in no
598 significant relationship between ozone and Australian temperatures. However, there does not
599 seem to be as clear a difference between REF-C1 and REF-C2 pairs in the four other CCMI
600 models that have an interactive ocean for REF-C2 (Fig. 5), and this hypothesis, therefore,
601 requires further investigation.

602 The second possibility is that the models are unable to represent the key processes
603 necessary to simulate the ozone-temperature relationship correctly. In the WACCM coupled
604 experiment, for example, significant correlations ($p < 0.1$) for November ozone and summer
605 surface temperatures in South-Southeast Australia are only obtained after linearly removing the
606 ENSO signal (not shown) and are still much weaker than observed (Table 1). As noted in
607 Section 3d, the large ENSO amplitude (Deser et al. 2012; Marsh et al. 2013) in the WACCM
608 coupled model may be interfering with the SAM response and impacting the relationship
609 between ozone and surface climate. Furthermore, in the coupled experiment, sea ice is
610 interactive (compared to the uncoupled experiment where it is prescribed from observations);
611 therefore, it is also possible that the coupled model could be influenced by a sea ice feedback
612 (Magnusdottir et al. 2004) that may interfere with the SAM. The preliminary analysis of the
613 fixed GHG experiments (Section 3b) highlights that the coupled model shows an improved
614 simulation of the ozone-surface temperature relationship when the long-term warming
615 associated with increased GHGs is omitted. This suggests that the warming acts to interfere
616 with the interannual variability in ozone and surface climate relationship in the coupled
617 experiment. One hypothesis is that the unrealistic Antarctic sea ice declines and different SST

patterns could push the climate system into a different state to that observed and will be the subject of future work.

The third possibility is that the observed connection between ozone and Australian temperatures is not particularly robust. While Bandoro et al. (2014) reported a statistically significant relationship between November Halley ozone and ERA-Interim summer surface temperatures in Eastern Australia, correlations are largest when these two datasets are used and are weaker or more variable for other combinations. The correlations in this study for the period 1979-2004 are also weaker overall than for 1979-2012 (not shown). After 2000 the TCO trend is less negative and even starting to become positive due to initial signs of ozone recovery (WMO 2014; Solomon et al. 2016), although detection of recovery is hindered by limited data records and large atmospheric variability (Chipperfield et al. 2017). Studies have linked the summer positive SAM trend since 2000 to recent changes in SSTs and decadal variability (Pacific decadal oscillation, e.g., Schneider et al. 2015) in addition to ozone depletion and these changes could also be influencing the observed relationship. The possible time-varying nature in the strength of the ozone-temperature connection makes it difficult to compare the observations to model output directly. Further analysis is required to examine the strength and linearity of this relationship and its applicability to additional datasets, to assess whether model results fall within error estimates.

b. Predicting Australian summer temperatures with ozone

This study aimed to examine whether interannual Antarctic spring ozone variability could be used as an indicator of Australian summer surface temperature variability in climate models. To this end, this work has shown that some CCMs can capture the observed relationship between ozone and surface temperatures, and has, therefore, indicated a potential benefit of incorporating ozone variability in seasonal forecasting systems. Operational seasonal

643 forecasting systems such as the Australian Bureau of Meteorology's seasonal climate forecast
644 system, Predictive Ocean and Atmosphere Model for Australia (POAMA), are coupled but
645 initialised with observed atmosphere and ocean conditions (Lim et al. 2016). Therefore, the
646 ability of some uncoupled models in this study, including WACCM (Fig. 5), to capture a strong
647 relationship between ozone and Australian summer surface temperatures is encouraging to
648 eventually use real-time ozone variability to improve skill in season outlook systems. However,
649 the reliability and accuracy of modelling this relationship is hindered by model biases. Further
650 research to assess model biases will assist in understanding why some models cannot correctly
651 simulate this observed connection with a view to eliminating model biases and eventually
652 improving seasonal prediction.

653 Current operational seasonal forecasting models typically have a poorly resolved
654 stratosphere (Maycock et al. 2011). For example, POAMA only has five levels above 200 hPa,
655 and the ozone concentration is set to climatological values (Lim et al. 2016). It may be unable
656 to capture links between the stratosphere and troposphere, and thus, there is a large scope for
657 improving prediction of tropospheric interannual variability. Roff et al. (2011) found that
658 improvements in the stratosphere in a forecasting model, such as a higher stratospheric
659 resolution and better representation of stratospheric dynamics and thermodynamics, led to
660 significant improvements in tropospheric forecast skill. Hence, even if spring Antarctic ozone
661 levels do not prove to be a reliable predictor of SH summer temperature extremes, there is still
662 potential benefit in including time-varying ozone and improving stratospheric representation in
663 operational forecasting systems.

664

665 **5. Conclusions**

666 This study examined the ability for WACCM as well as other CCMs to simulate
667 observed links between the spring Antarctic ozone hole and summer surface temperatures over

Australia. A systematic difference is found between the uncoupled and coupled experiments in WACCM and three possible interpretations are provided to explain the discrepancy in simulating the ozone-temperature teleconnection: (1) SSTs play a dominant role and drive interannual variations in both the ozone hole and Australian temperatures, (2) the CCMI models are unable to represent key processes and/or (3) the observed relationship has some uncertainty and is time-varying. While the Australian temperatures and ozone hole may be responding primarily to the SSTs in WACCM, there is some indication that CCMI uncoupled experiments also capture the relationship with more fidelity than the coupled experiments. However, there is not as clear a difference between other coupled and uncoupled experiment pairs amongst the CCMI models, and this hypothesis requires further investigation. It is also possible that the models are unable to capture the observed relationship due to biases, such as in the ENSO amplitude. Furthermore, long-term GHG-induced warming also seems to interfere with the response in the WACCM coupled model. This paper has also highlighted that there is some observational uncertainty regarding the strength of the ozone-temperature teleconnection.

The results of this study are encouraging for incorporating ozone variability to improve seasonal predictions, though more work is needed to identify causality in the link between spring ozone and SH surface climate. An experiment that compares the predictive skill in a seasonal forecasting model that is initialised with and without observed ozone would be the next step to demonstrating useful seasonal skill from Antarctic ozone. In addition, targeted modelling experiments which separate the role of SSTs and interannual ozone variations would help to elucidate the mechanism by which ozone impacts the surface climate.

Acknowledgements.

Zoe Gillett was funded by the Grains Research and Development Corporation (UHS11005). Portions of this study were supported by the Regional and Global Climate

693 Modeling Program (RGCM) of the U.S. Department of Energy's Office of Biological and
694 Environmental Research (BER) Cooperative agreement DE-FC02-97ER62402 and the
695 National Science Foundation (NSF) as well as the Australian Research Council (ARC) Centre
696 of Excellence for Climate Extremes (CE170100023). Andrea Dittus acknowledges support
697 from the ARC Centre of Excellence for Climate System Science (CE110001028) and the UK
698 National Environment Research Council (NERC) Project SMURPHS (NE/N006054/1).

699 This research was undertaken with the assistance of resources and services from the
700 National Computational Infrastructure, which is supported by the Australian Government. The
701 National Center for Atmospheric Research (NCAR) Command Language (NCL; NCL 2017)
702 was used for data analysis and visualisation.

703 We acknowledge the modelling groups for making their simulations available for this
704 analysis, the joint WCRP SPARC/IGAC Chemistry-Climate Model Initiative (CCMI) for
705 organising and coordinating the model data analysis activity, and the British Atmospheric Data
706 Centre (BADC) for collecting and archiving the CCMI model output. We acknowledge high-
707 performance computational support for the WACCM simulations from Yellowstone
708 (ark:/85065/d7wd3xhc) provided by the Climate Simulation Laboratory at NCAR's
709 Computational and Information Systems Laboratory, sponsored by NSF and other agencies.
710 NCAR is funded by NSF. Robyn Schofield and Kane Stone acknowledge support from the
711 ARC Centre of Excellence for Climate System Science (CE110001028), the Australian
712 Government's National Computational Merit Allocation Scheme (q90) and Australian
713 Antarctic science grant program (FoRCES 4012). The EMAC simulations have been performed
714 at the German Climate Computing Centre (DKRZ) through support from the
715 Bundesministerium für Bildung und Forschung (BMBF). DKRZ and its scientific steering
716 committee are gratefully acknowledged for providing the HPC and data archiving resources for
717 the consortial project ESCiMo (Earth System Chemistry integrated Modelling). Eugene

718 Rozanov acknowledges partial support from the Swiss National Science Foundation under
719 grants 200021 169241 (VEC) and 200020 182239 (POLE) and the gained information will be
720 used to improve the CCM SOCOL. We also acknowledge Bodeker Scientific, supported
721 through the Deep South National Science Challenge, for providing the combined total column
722 ozone database.
723 We thank Dan Marsh for useful discussions during the course of this study, and three
724 anonymous reviewers whose comments helped to significantly improve the manuscript.
725
726 APPENDIX
727 **Ozone index standard deviation**
728
729 APPENDIX B
730 **SAM index standard deviation**
731
732 **References**

733 Arblaster, J. M., and G. A. Meehl, 2006: Contributions of External Forcings to Southern
734 Annular Mode Trends. *J. Climate*, **19,** 2896-2905, doi:10.1175/jcli3774.1.

735 Arblaster, J. M., and L. V. Alexander, 2012: The impact of the El Niño-Southern Oscillation
736 on maximum temperature extremes. *Geophys. Res. Lett.*, **39,** 5,
737 doi:10.1029/2012gl053409.

738 Bandoro, J., S. Solomon, A. Donohoe, D. W. J. Thompson, and B. D. Santer, 2014:
739 Influences of the Antarctic Ozone Hole on Southern Hemispheric Summer Climate
740 Change. *J. Climate*, **27,** 6245-6264, doi:10.1175/JCLI-D-13-00698.1.

741 Bodeker, G. E., H. Shiona, and H. Eskes, 2005: Indicators of Antarctic ozone depletion.
742 *Atmos. Chem. Phys.*, **5,** 2603-2615.

743 Bretherton, C. S., M. Widmann, V. P. Dymnikov, J. M. Wallace, and I. Blade, 1999: The
744 effective number of spatial degrees of freedom of a time-varying field. *J. Climate*, **12,**
745 1990-2009, doi:10.1175/1520-0442(1999)012<1990:tenosd>2.0.co;2.

746 Chipperfield, M. P., and Coauthors, 2017: Detecting recovery of the stratospheric ozone
747 layer. *Nature*, **549,** 211-218, doi:10.1038/nature23681.

748 Dee, D. P., and Coauthors, 2011: The ERA-Interim reanalysis: configuration and performance
749 of the data assimilation system. *Quart. J. Roy. Meteor. Soc.*, **137,** 553-597,
750 doi:10.1002/qj.828.

751 Dennison, F. W., A. J. McDonald, and O. Morgenstern, 2015: The effect of ozone depletion
752 on the Southern Annular Mode and stratosphere-troposphere coupling. *J. Geophys.*
753 *Res.*, **120,** 6305-6312, doi:10.1002/2014jd023009.

754 Deser, C., and Coauthors, 2012: ENSO and Pacific Decadal Variability in the Community
755 Climate System Model Version 4. *J. Climate*, **25,** 2622-2651, doi:10.1175/jcli-d-11-
756 00301.1.

757 Ding, Q. H., E. J. Steig, D. S. Battisti, and J. M. Wallace, 2012: Influence of the Tropics on
758 the Southern Annular Mode. *J. Climate*, **25,** 6330-6348, doi:10.1175/jcli-d-11-
759 00523.1.

760 Eyring, V., and Coauthors, 2006: Assessment of temperature, trace species, and ozone in
761 chemistry-climate model simulations of the recent past. *J. Geophys. Res.,* **111,**
762 D22308, doi:10.1029/2006jd007327.

763 Eyring, V., and Coauthors, 2013: Overview of IGAC/SPARC Chemistry-Climate Model
764 Initiative (CCMI) community simulations in support of upcoming ozone and climate
765 assessments. *SPARC Newsletter*, **40,** 48-66.

766 Fogt, R. L., J. Perlwitz, S. Pawson, and M. A. Olsen, 2009: Intra-annual relationships between
767 polar ozone and the SAM. *Geophys. Res. Lett.*, **36,** L04707,
768 doi:10.1029/2008gl036627.

769 Gillett, N. P., and D. W. J. Thompson, 2003: Simulation of Recent Southern Hemisphere
770 Climate Change. *Science*, **302,** 273-275, doi:10.1126/science.1087440.

771 Gong, D., and S. Wang, 1999: Definition of Antarctic Oscillation index. *Geophys. Res. Lett.*,
772 **26,** 459-462, doi:10.1029/1999GL900003.

773 Grise, K. M., and L. M. Polvani, 2017: Understanding the Time Scales of the Tropospheric
774 Circulation Response to Abrupt CO2 Forcing in the Southern Hemisphere:
775 Seasonality and the Role of the Stratosphere. *J. Climate*, **30,** 8497-8515,
776 doi:10.1175/jcli-d-16-0849.1.

777 Hendon, H. H., D. W. J. Thompson, and M. C. Wheeler, 2007: Australian rainfall and surface
778 temperature variations associated with the Southern Hemisphere annular mode. *J.*
779 *Climate*, **20,** 2452-2467, doi:10.1175/jcli4134.1.

780 Hudson, D., A. G. Marshall, O. Alves, G. Young, D. Jones, and A. Watkins, 2016:
781 Forewarned is Forearmed: Extended-Range Forecast Guidance of Recent Extreme
782 Heat Events in Australia. *Wea. Forecasting*, **31,** 697-711, doi:10.1175/waf-d-15-
783 0079.1.

784 Ivy, D. J., C. Hilgenbrink, D. Kinnison, R. A. Plumb, A. Sheshadri, S. Solomon, and D. W. J.
785 Thompson, 2017: Observed Changes in the Southern Hemispheric Circulation in May.
786 *J. Climate*, **30,** 527-536, doi:10.1175/jcli-d-16-0394.1.

787 Jones, D. A., W. Wang, and R. Fawcett, 2009: High-quality spatial climate data-sets for
788 Australia. *Aust. Meteor. Oceanogr. J.*, **58,** 233-248.

789 Karoly, D. J., 1989: Southern Hemisphere Circulation Features Associated with El Niño-
790 Southern Oscillation Events. *J. Climate*, **2,** 1239-1252, doi:10.1175/1520-
791 0442(1989)002<1239:shcfaw>2.0.co;2.

792 Kidston, J., A. S. Taschetto, D. W. J. Thompson, and M. H. England, 2011: The influence of
793 Southern Hemisphere sea-ice extent on the latitude of the mid-latitude jet stream.
794 *Geophys. Res. Lett.*, **38,** 5, doi:10.1029/2011gl048056.

795 L'Heureux, M. L., and D. W. J. Thompson, 2006: Observed relationships between the El
796 Niño-Southern Oscillation and the extratropical zonal-mean circulation. *J. Climate*,
797 **19,** 276-287, doi:10.1175/jcli3617.1.

798 Lee, S., and S. B. Feldstein, 2013: Detecting Ozone- and Greenhouse Gas-Driven Wind
799 Trends with Observational Data. *Science*, **339,** 563-567, doi:10.1126/science.1225154.

800 Li, F., P. A. Newman, and R. S. Stolarski, 2010: Relationships between the Brewer-Dobson
801 circulation and the southern annular mode during austral summer in coupled
802 chemistry-climate model simulations. *J. Geophys. Res.*, **115,** 12,
803 doi:10.1029/2009jd012876.

804 Li, F., Y. V. Vikhliaev, P. A. Newman, S. Pawson, J. Perlwitz, D. W. Waugh, and A. R.
805 Douglass, 2016: Impacts of Interactive Stratospheric Chemistry on Antarctic and

Southern Ocean Climate Change in the Goddard Earth Observing System, Version 5 (GEOS-5). *J. Climate*, **29,** 3199-3218, doi:10.1175/jcli-d-15-0572.1.

Lim, E.-P., H. H. Hendon, and H. Rashid, 2013: Seasonal Predictability of the Southern Annular Mode due to Its Association with ENSO. *J. Climate*, **26,** 8037-8054, doi:10.1175/jcli-d-13-00006.1.

Lim, E.-P., and H. H. Hendon, 2015: Understanding the Contrast of Australian Springtime Rainfall of 1997 and 2002 in the Frame of Two Flavors of El Niño. *J. Climate*, **28,** 2804-2822, doi:10.1175/jcli-d-14-00582.1.

Lim, E.-P., H. H. Hendon, D. Hudson, M. Zhao, L. Shi, O. Alves, and G. Young, 2016: Evaluation of the ACCESS-S1 hindcasts for prediction of Victorian seasonal rainfall. *Bureau Research Report*, **19**.

Lim, E. P., H. H. Hendon, and D. W. J. Thompson, 2018: Seasonal Evolution of Stratosphere-Troposphere Coupling in the Southern Hemisphere and Implications for the Predictability of Surface Climate. *J. Geophys. Res.*, **123,** 12,002-12,016, doi:10.1029/2018JD029321.

Lin, P., D. Paynter, L. Polvani, G. J. P. Correa, Y. Ming, and V. Ramaswamy, 2017: Dependence of model-simulated response to ozone depletion on stratospheric polar vortex climatology. *Geophys. Res. Lett.*, **44,** 6391-6398, doi:10.1002/2017gl073862.

Magnusdottir, G., C. Deser, and R. Saravanan, 2004: The effects of North Atlantic SST and sea ice anomalies on the winter circulation in CCM3. Part I: Main features and storm track characteristics of the response. *J. Climate*, **17,** 857-876, doi:10.1175/1520-0442(2004)017<0857:teonas>2.0.co;2.

828 Marsh, D. R., M. J. Mills, D. E. Kinnison, J.-F. Lamarque, N. Calvo, and L. M. Polvani,
829 2013: Climate Change from 1850 to 2005 Simulated in CESM1(WACCM). *J.*
830 *Climate*, **26,** 7372-7391, doi:10.1175/jcli-d-12-00558.1.

831 Marshall, G. J., 2003: Trends in the Southern Annular Mode from Observations and
832 Reanalyses. *J. Climate*, **16,** 4134-4143, doi:10.1175/1520-
833 0442(2003)016<4134:titsam>2.0.co;2.

834 Maycock, A. C., S. P. E. Keeley, A. J. Charlton-Perez, and F. J. Doblas-Reyes, 2011:
835 Stratospheric circulation in seasonal forecasting models: implications for seasonal
836 prediction. *Climate Dyn.*, **36,** 309-321, doi:10.1007/s00382-009-0665-x.

837 McBride, J. L., and N. Nicholls, 1983: Seasonal Relationships between Australian Rainfall
838 and the Southern Oscillation. *Mon. Wea. Rev.*, **111,** 1998-2004, doi:10.1175/1520-
839 0493(1983)111<1998:SRBARA>2.0.CO;2.

840 McCormick, M. P., L. W. Thomason, and C. R. Trepte, 1995: Atmospheric effects of the Mt
841 Pinatubo eruption. *Nature*, **373,** 399-404, doi:10.1038/373399a0.

842 McLandress, C., T. G. Shepherd, J. F. Scinocca, D. A. Plummer, M. Sigmond, A. I. Jonsson,
843 and M. C. Reader, 2011: Separating the Dynamical Effects of Climate Change and
844 Ozone Depletion. Part II: Southern Hemisphere Troposphere. *J. Climate*, **24,** 1850-
845 1868, doi:10.1175/2010jcli3958.1.

846 Meinshausen, M., and Coauthors, 2011: The RCP greenhouse gas concentrations and their
847 extensions from 1765 to 2300. *Climatic Change*, **109,** 213, doi:10.1007/s10584-011-
848 0156-z.

849 Min, S. K., W. Cai, and P. Whetton, 2013: Influence of climate variability on seasonal
850 extremes over Australia. *J. Geophys. Res.*, **118,** 643-654, doi:10.1002/jgrd.50164.

851 Mo, K. C., 2000: Relationships between low-frequency variability in the Southern
852 Hemisphere and sea surface temperature anomalies. *J. Climate*, **13,** 3599-3610,
853 doi:10.1175/1520-0442(2000)013<3599:rblfvi>2.0.co;2.

854 Morgenstern, O., and Coauthors, 2017: Review of the global models used within phase 1 of
855 the Chemistry-Climate Model Initiative (CCMI). *Geosci. Model Dev.*, **10,** 639-671,
856 doi:10.5194/gmd-10-639-2017.

857 Perkins, S. E., D. Argueso, and C. J. White, 2015: Relationships between climate variability,
858 soil moisture, and Australian heatwaves. *J. Geophys. Res.*, **120,** 8144-8164,
859 doi:10.1002/2015jd023592.

860 Perkins-Kirkpatrick, S. E., and Coauthors, 2016: Natural hazards in Australia: heatwaves.
861 *Climatic Change*, **139,** 101-114, doi:10.1007/s10584-016-1650-0.

862 Polvani, L. M., D. W. Waugh, G. J. P. Correa, and S. W. Son, 2011: Stratospheric Ozone
863 Depletion: The Main Driver of Twentieth-Century Atmospheric Circulation Changes
864 in the Southern Hemisphere. *J. Climate*, **24,** 795-812, doi:10.1175/2010jcli3772.1.

865 Raphael, M. N., 2004: A zonal wave 3 index for the Southern Hemisphere. *Geophys. Res.*
866 *Lett.*, **31,** 4, doi:10.1029/2004gl020365.

867 Raphael, M. N., W. Hobbs, and I. Wainer, 2011: The effect of Antarctic sea ice on the
868 Southern Hemisphere atmosphere during the southern summer. *Climate Dyn.*, **36,**
869 1403-1417, doi:10.1007/s00382-010-0892-1.

870 Rayner, N. A., D. E. Parker, E. B. Horton, C. K. Folland, L. V. Alexander, D. P. Rowell, E.
871 C. Kent, and A. Kaplan, 2003: Global analyses of sea surface temperature, sea ice, and
872 night marine air temperature since the late nineteenth century. *J. Geophys. Res.*, **108,**
873 4407, doi:10.1029/2002JD002670.

874 Risbey, J. S., M. J. Pook, P. C. McIntosh, M. C. Wheeler, and H. H. Hendon, 2009: On the
875 Remote Drivers of Rainfall Variability in Australia. *Mon. Wea. Rev.*, **137,** 3233-3253,
876 doi:10.1175/2009mwr2861.1.

877 Roff, G., D. W. J. Thompson, and H. Hendon, 2011: Does increasing model stratospheric
878 resolution improve extended-range forecast skill? *Geophys. Res. Lett.*, **38,** L05809,
879 doi:10.1029/2010GL046515.

880 Rogers, J. C., and H. van Loon, 1982: Spatial Variability of Sea Level Pressure and 500 mb
881 Height Anomalies over the Southern Hemisphere. *Mon. Wea. Rev.*, **110,** 1375-1392,
882 doi:10.1175/1520-0493(1982)110<1375:svoslp>2.0.co;2.

883 Salby, M. L., E. A. Titova, and L. Deschamps, 2011: Rebound of Antarctic ozone. *Geophys.*
884 *Res. Lett.*, **38,** L09702, doi:10.1029/2011gl047266.

885 Salby, M. L., E. A. Titova, and L. Deschamps, 2012: Changes of the Antarctic ozone hole:
886 Controlling mechanisms, seasonal predictability, and evolution. *J. Geophys. Res.*, **117,**
887 D10111, doi:10.1029/2011jd016285.

888 Santer, B. D., T. M. L. Wigley, J. S. Boyle, D. J. Gaffen, J. J. Hnilo, D. Nychka, D. E. Parker,
889 and K. E. Taylor, 2000: Statistical significance of trends and trend differences in
890 layer-average atmospheric temperature time series. *J. Geophys. Res.*, **105,** 7337-7356,
891 doi:10.1029/1999jd901105.

892 Schneider, D. P., C. Deser, and T. T. Fan, 2015: Comparing the Impacts of Tropical SST
893 Variability and Polar Stratospheric Ozone Loss on the Southern Ocean Westerly
894 Winds. *J. Climate*, **28,** 9350-9372, doi:10.1175/jcli-d-15-0090.1.

895 Seviour, W. J. M., S. C. Hardiman, L. J. Gray, N. Butchart, C. MacLachlan, and A. A. Scaife,
896 2014: Skillful Seasonal Prediction of the Southern Annular Mode and Antarctic
897 Ozone. *J. Climate*, **27,** 7462-7474, doi:10.1175/jcli-d-14-00264.1.

898 Seviour, W. J. M., D. W. Waugh, L. M. Polvani, G. J. P. Correa, and C. I. Garfinkel, 2017:
899 Robustness of the Simulated Tropospheric Response to Ozone Depletion. *J. Climate*,
900 **30,** 2577-2585, doi:10.1175/jcli-d-16-0817.1.

901 Shaw, T. A., J. Perlwitz, N. Harnik, P. A. Newman, and S. Pawson, 2011: The Impact of
902 Stratospheric Ozone Changes on Downward Wave Coupling in the Southern
903 Hemisphere. *J. Climate*, **24,** 4210-4229, doi:10.1175/2011jcli4170.1.

904 Sheshadri, A., and R. A. Plumb, 2016: Sensitivity of the surface responses of an idealized
905 AGCM to the timing of imposed ozone depletion-like polar stratospheric cooling.
906 *Geophys. Res. Lett.*, **43,** 2330-2336, doi:10.1002/2016gl067964.

907 Smith, K. L., and L. M. Polvani, 2017: Spatial patterns of recent Antarctic surface
908 temperature trends and the importance of natural variability: lessons from multiple
909 reconstructions and the CMIP5 models. *Climate Dyn.*, **48,** 2653-2670,
910 doi:10.1007/s00382-016-3230-4.

911 Solomon, S., 1999: Stratospheric ozone depletion: A review of concepts and history. *Rev.*
912 *Geophys.*, **37,** 275-316, doi:10.1029/1999rg900008.

913 Solomon, S., D. J. Ivy, D. Kinnison, M. J. Mills, R. R. Neely, III, and A. Schmidt, 2016:
914 Emergence of healing in the Antarctic ozone layer. *Science*, **353,** 269-274,
915 doi:10.1126/science.aae0061.

916 Son, S.-W., and Coauthors, 2008: The Impact of Stratospheric Ozone Recovery on the
917 Southern Hemisphere Westerly Jet. *Science*, **320,** 1486-1489,
918 doi:10.1126/science.1155939.

919 Son, S.-W., A. Purich, H. H. Hendon, B.-M. Kim, and L. M. Polvani, 2013: Improved
920 seasonal forecast using ozone hole variability? *Geophys. Res. Lett.*, **40,** 6231-6235,
921 doi:10.1002/2013gl057731.

922 Stone, K. A., O. Morgenstern, D. J. Karoly, A. R. Klekociuk, W. J. French, N. L. Abraham,
923 and R. Schofield, 2016: Evaluation of the ACCESS - chemistry-climate model for the
924 Southern Hemisphere. *Atmos. Chem. Phys.*, **16,** 2401-2415, doi:10.5194/acp-16-2401-
925 2016.

926 Stone, K. A., and Coauthors, 2017: Observing the Impact of Calbuco Volcanic Aerosols on
927 South Polar Ozone Depletion in 2015. *J. Geophys. Res.*, **122,** 11862-11879,
928 doi:10.1002/2017JD026987.

929 Thompson, D. W. J., and S. Solomon, 2002: Interpretation of recent Southern Hemisphere
930 climate change. *Science*, **296,** 895-899, doi:10.1126/science.1069270.

931 Thompson, D. W. J., M. P. Baldwin, and S. Solomon, 2005: Stratosphere-troposphere
932 coupling in the Southern Hemisphere. *J. Atmos. Sci.*, **62,** 708-715, doi:10.1175/jas-
933 3321.1.

934 Thompson, D. W. J., S. Solomon, P. J. Kushner, M. H. England, K. M. Grise, and D. J.
935 Karoly, 2011: Signatures of the Antarctic ozone hole in Southern Hemisphere surface
936 climate change. *Nat. Geosci.*, **4,** 741-749, doi:10.1038/ngeo1296.

937 Trenberth, K. E., 1979: Interannual Variability of the 500 mb Zonal Mean Flow in the
938 Southern Hemisphere. *Mon. Wea. Rev.*, **107,** 1515-1524, doi:10.1175/1520-
939 0493(1979)107<1515:ivotmz>2.0.co;2.

940 Trenberth, K. E., 1997: The Definition of El Niño. *Bull. Amer. Meteor. Soc.*, **78,** 2771-2777,
941 doi:10.1175/1520-0477(1997)078<2771:tdoeno>2.0.co;2.

942 Turner, J., J. S. Hosking, T. J. Bracegirdle, T. Phillips, and G. J. Marshall, 2017: Variability
943 and trends in the Southern Hemisphere high latitude, quasi-stationary planetary waves.
944 *Int. J. Climatol.*, **37,** 2325-2336, doi:10.1002/joc.4848.

945 van Ommen, T. D., and V. Morgan, 2010: Snowfall increase in coastal East Antarctica linked
946 with southwest Western Australian drought. *Nat. Geosci.*, **3,** 267-272,
947 doi:10.1038/ngeo761.

948 World Meteorological Organization (WMO), 2014: Scientific Assessment of Ozone
949 Depletion: 2014, 416 pp.

950 Zubiaurre, I., and N. Calvo, 2012: The El Niño-Southern Oscillation (ENSO) Modoki signal
951 in the stratosphere. *J. Geophys. Res.*, **117,** 15, doi:10.1029/2011jd016690.
952
953
954
955
956

957 **LIST OF TABLES**

958 **Table 1.** Correlations coefficients for detrended November ozone and detrended summer
959 surface temperature over Eastern Australia from 1979-2004 in the WACCM
960 experiments. The correlations are calculated after first concatenating the 5 (3)
961 ensemble members from the uncoupled (coupled) experiment, apart from the
962 volcano analysis where the years corresponding to the El Chichón (1982) and
963 Mount Pinatubo (1991) eruptions were removed from the model ensemble
964 mean. Correlations for the concatenated members are also shown; refer to Fig.
965 5 for the ensemble mean values.
966 An asterisk indicates correlations statistically significant at the 90% confidence
967 level, italics for the 95% level and bold for the 99% level. A two-tailed *t* test is
968 used to test significance with the degrees of freedom reduced based on the lag-
969 1 autocorrelation. 43
970
971 **Table 2.** Correlation coefficients for detrended November ozone with the detrended
972 summer Niño 3.4 index, for the period 1979-2004. An asterisk indicates
973 correlations statistically significant at the 90% level, italics for the 95% level
974 and bold for the 99% level.. 44
975
976 **Table 3.** Same as Table 2, but for the correlation between November ozone and the
977 summer SAM. 45
978
979 **Table 4.** Correlation coefficients for detrended summer ENSO and summer SAM indices
980 with detrended Eastern Australia summer surface temperature, for the period

1979-2004. An asterisk indicates correlations that are statistically significant at the 90% level, italics for the 95% level and bold for the 99% level. 46

Table A1. Standard deviation of the ozone index over 26 years of data, for the observed Halley and NIWA-BS datasets and the three uncoupled, coupled, GHG1960 and ODS1960 WACCM ensemble members. 1979-2004 for September-December and 1980-2005 for January-April. 47

Table A2. Standard deviation of the SAM index over 26 years of data for each three-month overlapping period, for the Marshall (2003) SAM index and the three uncoupled and coupled WACCM ensemble members. 1979-2004 for periods beginning in September-December and 1980-2005 for January-April. 48

TABLE 1. Correlation coefficients for detrended November ozone and detrended summer surface temperature over Eastern Australia from 1979-2004 in the WACCM experiments. The ensemble mean and ENSO were removed from the 5 (3) concatenated ensemble members from the uncoupled (coupled) experiment, and the two major volcanic eruptions (El Chichón (1982) and Mount Pinatubo (1991)) were removed from the model ensemble mean. Correlations for the concatenated members are also shown; refer to Fig. 5 for the ensemble mean values.

An asterisk indicates correlations statistically significant at the 90% confidence level, italics for the 95% level and bold for the 99% level. A two-tailed *t* test is used to test significance with the degrees of freedom reduced based on the lag-1 autocorrelation.

Correlations between ozone and surface temperature		
Concatenated members	Uncoupled	**0.41**
	Coupled	0.11
Ensemble mean removed from concatenated members	Uncoupled	0.03
	Coupled	-0.05
ENSO removed from concatenated members	Uncoupled	**0.34**
	Coupled	0.16
Volcanic eruptions removed from ensemble mean	Uncoupled	**0.67**
	Coupled	0.08

TABLE 2. Correlation coefficients for detrended November ozone with the detrended summer Niño 3.4 index, for the period 1979-2004. An asterisk indicates correlations statistically significant at the 90% level, italics for the 95% level and bold for the 99% level.

Observations	Halley	0.11
	NIWA-BS	0.10
WACCM	Uncoupled	*0.26*
	Coupled	-0.03

TABLE 3. Same as Table 2, but for the correlation between November ozone and the summer SAM.

Observations	Halley	-0.33
	NIWA-BS	*-0.40*
WACCM	Uncoupled	**-0.30**
	Coupled	**-0.39**

TABLE 4. Correlation coefficients for detrended summer ENSO and summer SAM indices with detrended Eastern Australian summer surface temperature, for the period 1979-2004. An asterisk indicates correlations that are statistically significant at the 90% level, italics for the 95% level and bold for the 99% level.

Surface temperature correlated with ENSO and SAM		
ENSO	Observations	*0.39*
	Uncoupled	**0.47**
	Coupled	**0.61**
SAM	Observations	-0.24
	Uncoupled	**-0.41**
	Coupled	-0.03
	CCSM4	0.10
	CESM1-CAM5	**-0.36**

TABLE A1. Standard deviation of the ozone index over 26 years of data, for the observed Halley and NIWA-BS datasets and the three uncoupled, coupled, GHG1960 and ODS1960 WACCM ensemble members. 1979-2004 for September-December and 1980-2005 for January-April.

			Sep	Oct	Nov	Dec	Jan	Feb	Mar	Apr
Observations	Halley		19.61	33.14	43.86	21.86	8.40	8.53	10.41	14.11
	NIWA-BS		23.67	33.48	34.33	13.95	6.05	6.45	6.64	7.63
WACCM	Uncoupled	r1i1p1	24.38	31.88	32.92	22.90	11.36	9.43	8.36	8.81
		r2i1p1	27.13	32.47	29.12	22.07	12.71	10.19	9.35	8.79
		r3i1p1	29.37	33.14	28.58	22.03	13.41	9.31	8.53	8.15
	Coupled	r1i1p1	22.75	30.63	27.48	18.52	9.76	8.16	7.60	6.36
		r2i1p1	21.99	28.71	28.08	18.06	9.71	8.30	7.35	6.76
		r3i1p1	22.97	25.98	27.11	20.30	11.72	8.00	6.72	8.37
	GHG1960	r1i1p1	23.74	29.79	27.64	19.00	10.79	8.75	7.92	7.93
		r2i1p1	23.60	27.47	28.05	17.47	9.83	7.82	7.86	6.91
		r3i1p1	25.83	28.47	26.81	22.17	12.68	9.66	10.04	9.98
	ODS1960	r1i1p1	13.44	14.06	13.55	8.15	6.90	5.74	5.52	6.70
		r2i1p1	15.52	16.32	15.74	9.83	7.64	6.74	7.96	8.70
		r3i1p1	15.24	16.78	14.78	7.21	6.53	5.29	6.23	7.72

TABLE A2. Standard deviation of the SAM index over 26 years of data for each three-month overlapping period, for the Marshall (2003) SAM index and the three uncoupled and coupled WACCM ensemble members. 1979-2004 for periods beginning in September-December and 1980-2005 for January-April.

			SON	OND	NDJ	DJF	JFM	FMA	MAM	AMJ
Observations			1.26	1.29	1.15	1.10	1.00	1.02	1.05	1.06
WACCM	Uncoupled	r1i1p1	1.46	1.49	1.33	1.29	0.83	0.82	1.07	1.06
		r2i1p1	1.08	1.12	1.06	1.15	1.14	1.17	1.09	1.02
		r3i1p1	1.23	1.29	1.19	1.11	1.19	1.32	1.24	1.11
	Coupled	r1i1p1	1.13	1.09	1.07	1.11	1.27	1.13	1.27	1.14
		r2i1p1	1.06	1.05	1.05	1.16	0.93	0.79	0.72	1.16
		r3i1p1	0.99	1.01	1.08	1.07	0.83	0.93	1.16	1.13

1111 **LIST OF FIGURES**

1112 **Fig. 1.** Time series (1979-2004) of the November ozone index for the first ensemble member
1113 of WACCM (a) uncoupled (REF-C1) and (b) coupled (REF-C2) experiments, and the
1114 detrended November ozone index for (c) uncoupled and (d) coupled. Years with
1115 high/low polar cap (63-90°S) averaged TCO are identified as those that exceed +/- one
1116 standard deviation (red/blue horizontal lines). Note that +/- one standard deviation is
1117 calculated across the three members. 52
1118
1119 **Fig. 2.** Lag correlation between the detrended ozone index and detrended SAM index for each
1120 3-month overlapping period, for 1979-2004 (1980-2005 for the ozone index in January-
1121 April). (a) Halley ozone (75°S, 25°W) and (b) NIWA-BS ozone (63-90°S) with the
1122 Marshall (2003) SAM index, and (c), (d), (e) and (f) TCO (63-90°S) and SAM from
1123 WACCM uncoupled, coupled, GHG1960 and ODS1960 experiments, respectively. The
1124 horizontal axis indicates the ozone index month. The vertical axis shows the 3-month
1125 overlapping average SAM, e.g. September ozone correlated with SAM in +0 SON, +1
1126 OND, +2 NDJ, +3 DJF and +4 JFM. The correlation coefficients that are statistically
1127 significant at the 90%, 95% and 99% confidence levels are bound by yellow, green and
1128 white contour lines, respectively. A two-tailed *t* test is used to test significance, with the
1129 degrees of freedom reduced based on the lag-1 autocorrelation coefficient. 53
1130
1131 **Fig. 3.** As in Fig. 2, but for the lagged correlation between the ozone index and Eastern
1132 Australia surface temperature. Two surface temperature datasets are used for the
1133 observations: ERA-Interim for (a) with Halley ozone and (c) NIWA-BS ozone, and
1134 AWAP with (b) Halley and (d) NIWA-BS 55
1135

1136 **Fig. 4.** Correlation coefficients between detrended November ozone and detrended summer
1137 surface temperatures (1979-2004) for (a) Halley ozone and (b) NIWA-BS ozone with
1138 ERA-Interim surface temperatures, and (c) and (d) ozone and surface temperatures from
1139 WACCM uncoupled and coupled experiments, respectively. Hatching indicates
1140 correlations that are statistically significant at the 95% level. 57
1141
1142 **Fig. 5.** Correlation coefficients for detrended November ozone and detrended Eastern Australia
1143 summer surface temperature (1979-2004). Column 1 shows the observations: ERA-
1144 Interim surface temperature and Halley (red cross; 75°S, 26°W), Syowa (yellow; 69°S,
1145 39°E), South Pole (blue; 90°S, 25°W), and NIWA-BS (green; 63-90°S) ozone. Columns
1146 2 and 3 show the WACCM uncoupled and coupled experiments, respectively.
1147 Individual ensemble members are shown with a cross and the ensemble mean with a
1148 circle. Columns 4, 5 and 6 show all available members for the CCMI models in three
1149 groups: CCMI-REF-C1, CCMI-REF-C2-uncoupled where SSTs and sea ice are
1150 prescribed from another climate model, and CCMI-REF-C2-coupled (ACCESS-CCM
1151 = red cross, CESM1 CAM4-Chem = blue, CMAM = magenta, EMAC-L47MA = grey,
1152 EMAC-L90MA = dark green, GEOSCCM = purple, MRI-ESM = pale green, NIWA-
1153 UKCA = yellow, SOCOL = orange). 58
1154
1155 **Fig. 6.** Time-height evolution of the composite differences (high – low ozone) between the
1156 years with the highest and lowest (magnitude exceeds one standard deviation; number
1157 of years indicated at the top left of each column) polar cap (63-90°S) averaged
1158 November ozone values (1979-2004) for vertically resolved polar cap average
1159 geopotential height [m]. Left: composite differences for WACCM uncoupled

experiment; right: coupled experiment. Hatching indicates differences that are statistically significant at the 95% level. 60

Fig. 7. Composite differences (high – low ozone) in summer between the years with the highest and lowest (magnitude exceeds one standard deviation; number of years indicated at the top left of each column) November ozone values (1979-2004). (a, b) Surface temperature [K]. (c, d) Zonal wind at 500 hPa [m s^{-1}]. (e, f) Sea level pressure (SLP) [Pa]. Left: composite differences for Halley ozone; right: for NIWA-BS ozone. Hatching indicates differences that are statistically significant at the 95% level. 61

Fig. 8. As in Fig. 7, but for WACCM. Left: composite differences for the uncoupled experiment; right: for coupled experiment. 62

Fig. 9. Correlation coefficients between detrended Eastern Australia summer surface temperatures and detrended summer SSTs and SLP (1979-2004) for (a, b) observations, and (c, d) uncoupled and (e, f) coupled WACCM experiments. Hatching indicates correlations that are statistically significant at the 95% level. 63

Fig. 10. As in Figs. 7 and 8, but for the composite differences (high – low SAM) in summer between the positive and negative phases of the summer SAM (when the magnitude exceeds one standard deviation; number of years indicated at the top left of each column). (a, d, g) observations, and (b, e, h) uncoupled and (c, f, i) coupled WACCM experiments. 64

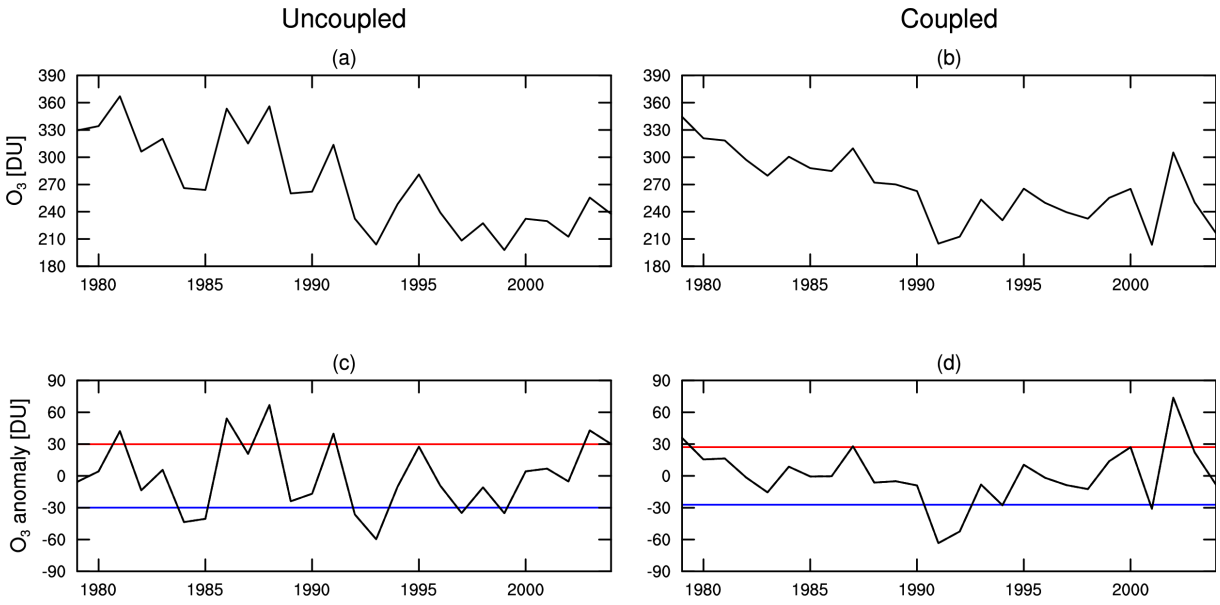

FIG. 1. Time series (1979-2004) of the November ozone index for the first ensemble member of WACCM (a) uncoupled (REF-C1) and (b) coupled (REF-C2) experiments, and the detrended November ozone index for (c) uncoupled and (d) coupled. Years with high/low polar cap (63-90°S) averaged TCO are identified as those that exceed +/- one standard deviation (red/blue horizontal lines). Note that +/- one standard deviation is calculated across the three members.

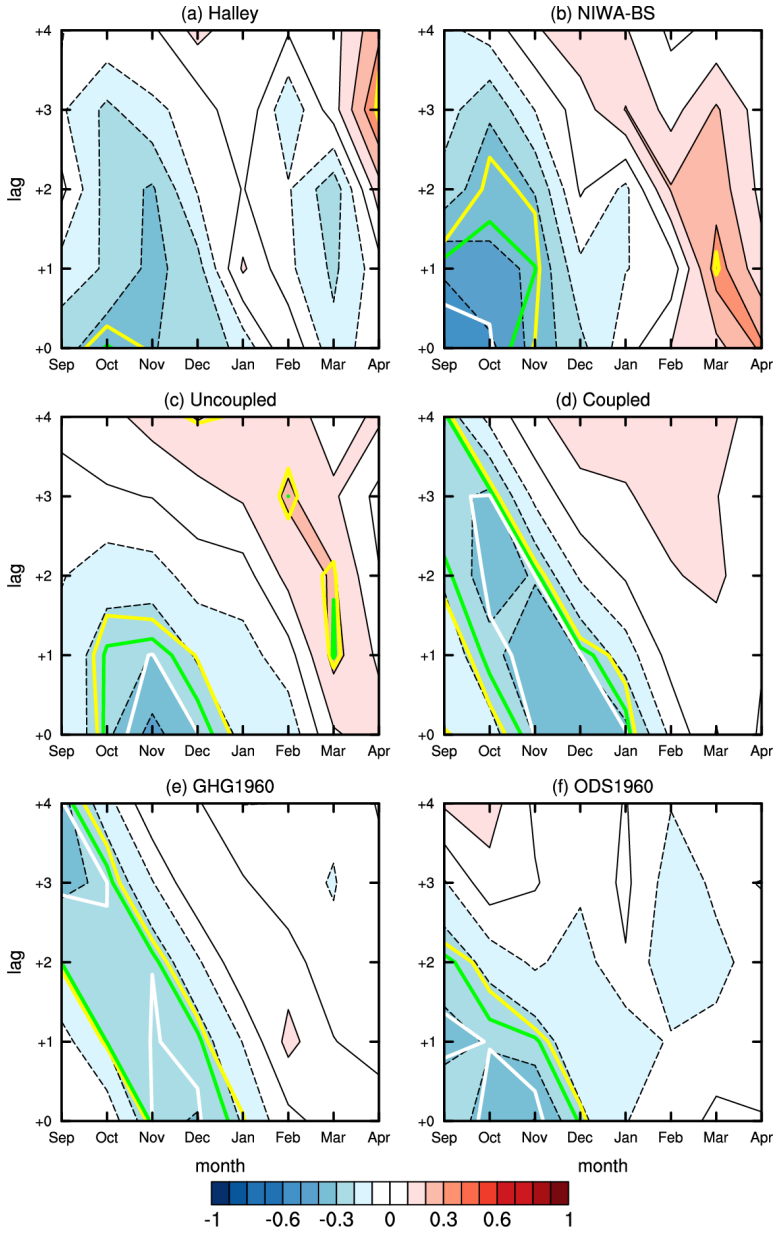

1198

1199 FIG. 2. Lag correlation between the detrended ozone index and detrended SAM index
1200 for each 3-month overlapping period, for 1979-2004 (1980-2005 for the ozone index in
1201 January-April). (a) Halley ozone (75°S, 25°W) and (b) NIWA-BS ozone (63-90°S) with the
1202 Marshall (2003) SAM index, and (c), (d), (e) and (f) TCO (63-90°S) and SAM from WACCM
1203 uncoupled, coupled, GHG1960 and ODS1960 experiments, respectively. The horizontal axis
1204 indicates the ozone index month. The vertical axis shows the 3-month overlapping average
1205 SAM, e.g. September ozone correlated with SAM in +0 SON, +1 OND, +2 NDJ, +3 DJF and
1206 +4 JFM. The correlation coefficients that are statistically significant at the 90%, 95% and 99%

confidence levels are bound by yellow, green and white contour lines, respectively. A two-tailed *t* test is used to test significance, with the degrees of freedom reduced based on the lag-1 autocorrelation coefficient.

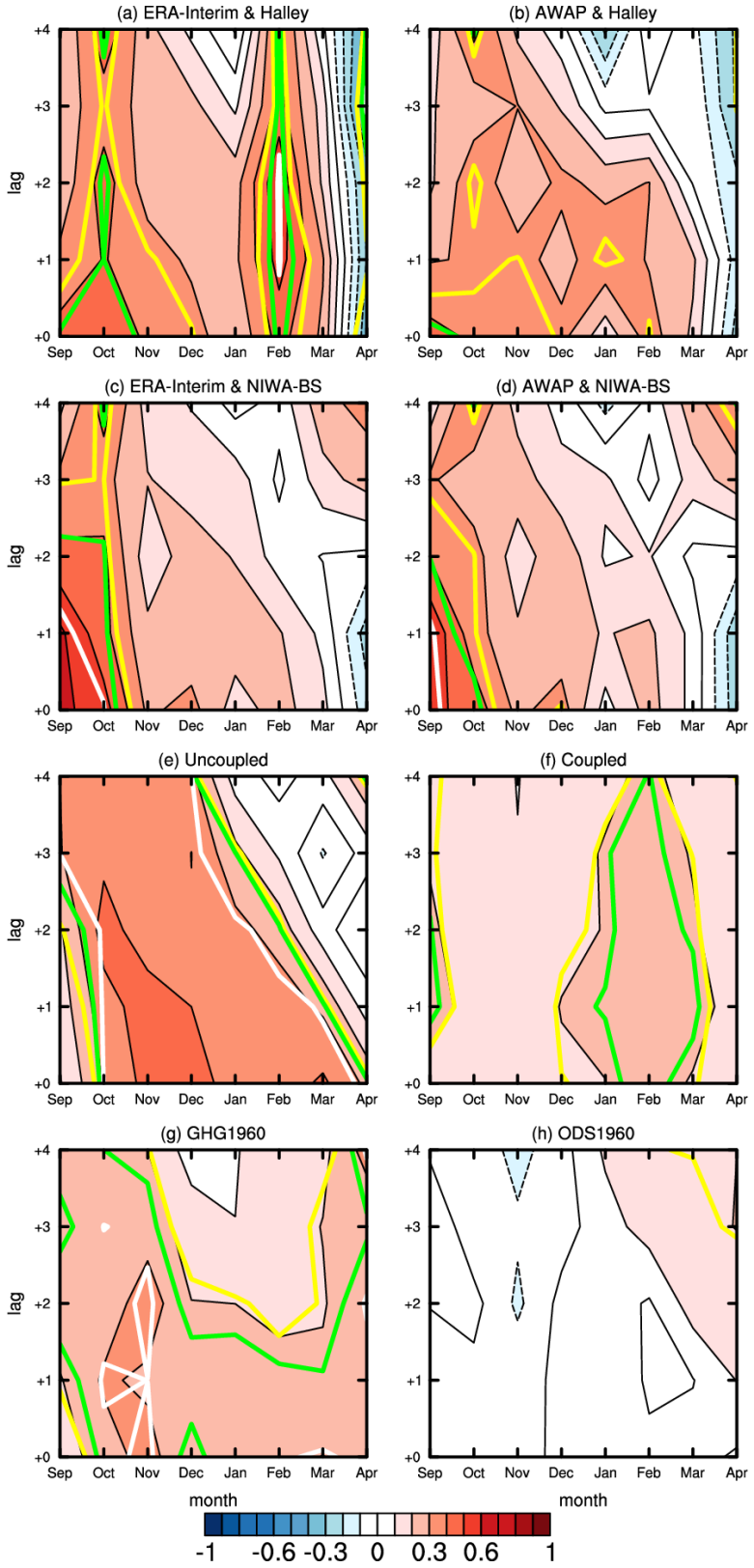

1210

1211 FIG. 3. As in Fig. 2, but for the lagged correlation between the ozone index and Eastern

1212 Australia surface temperature. Two surface temperature datasets are used for the observations:

ERA-Interim for (a) with Halley ozone and (c) NIWA-BS ozone, and AWAP with (b) Halley and (d) NIWA-BS.

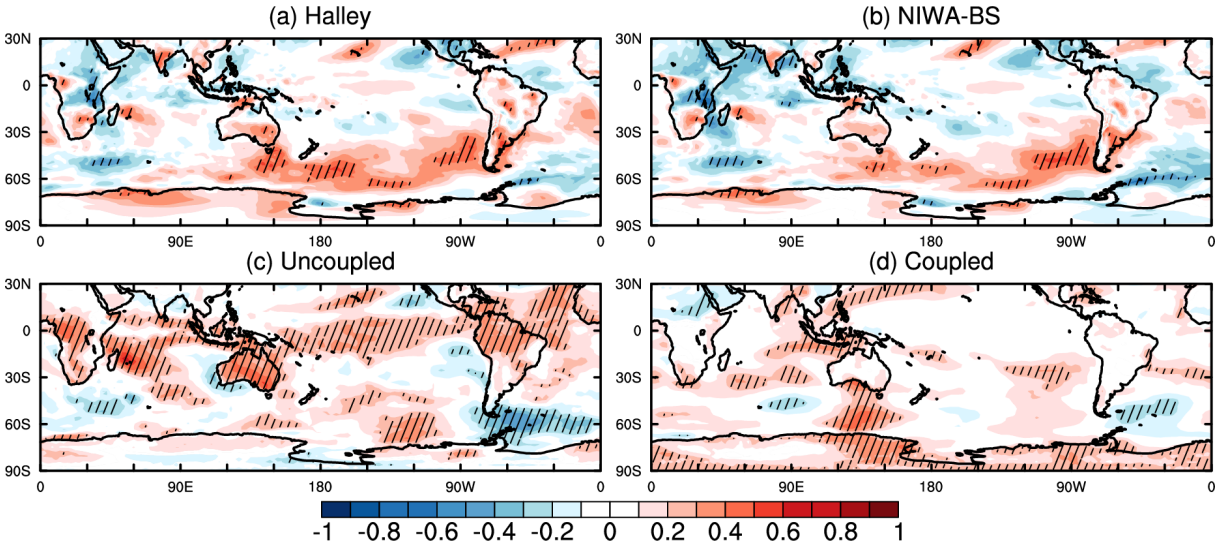

FIG. 4. Correlation coefficients between detrended November ozone and detrended summer surface temperatures (1979-2004) for (a) Halley ozone and (b) NIWA-BS ozone with ERA-Interim surface temperatures, and (c) and (d) ozone and surface temperatures from WACCM uncoupled and coupled experiments, respectively. Hatching indicates correlations that are statistically significant at the 95% level.

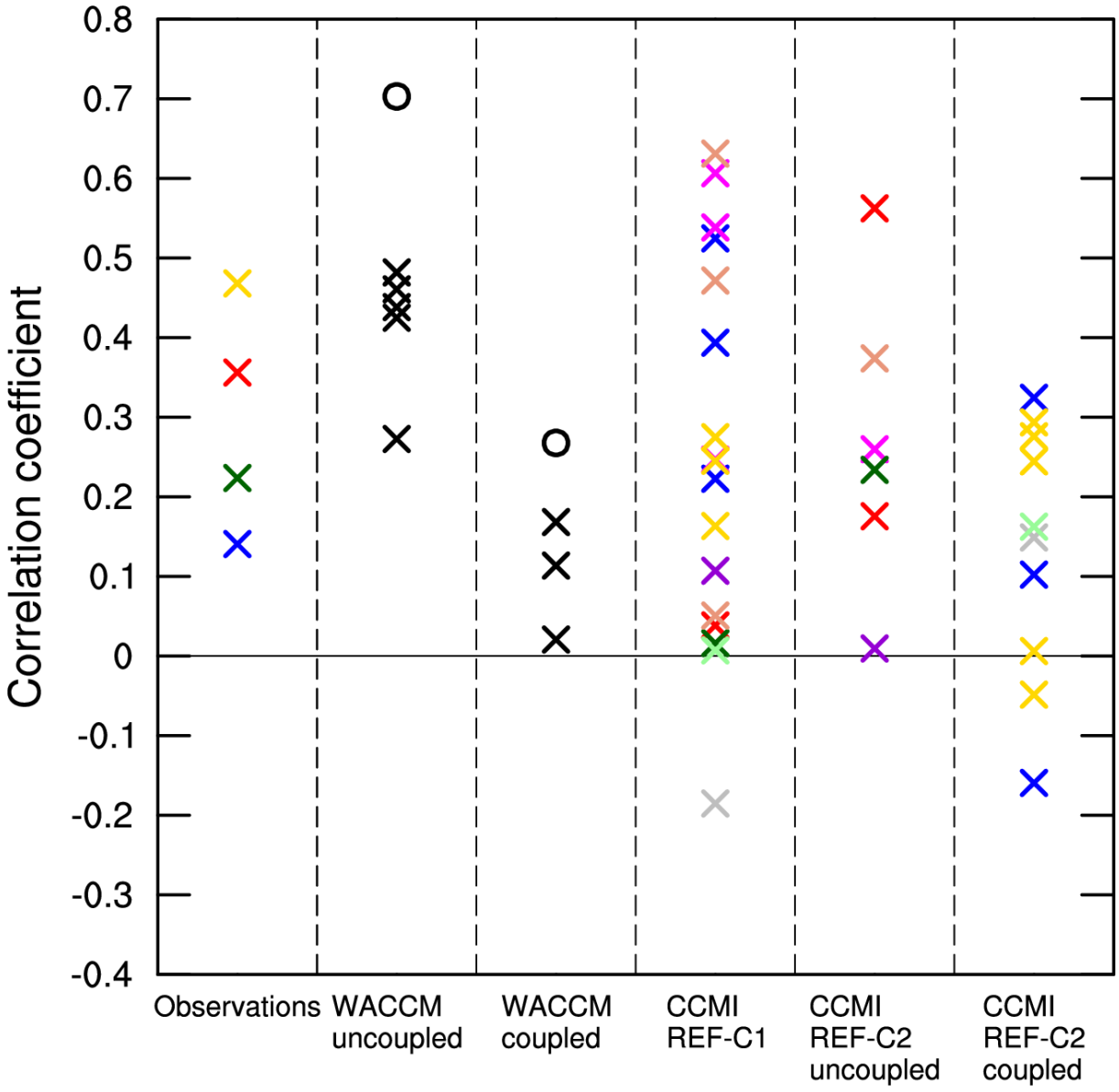

FIG. 5. Correlation coefficients for detrended November ozone and detrended Eastern Australia summer surface temperature (1979-2004). Column 1 shows the observations: ERA-Interim surface temperature and Halley (red cross; 75°S, 26°W), Syowa (yellow; 69°S, 39°E), South Pole (blue; 90°S, 25°W), and NIWA-BS (green; 63-90°S) ozone. Columns 2 and 3 show the WACCM uncoupled and coupled experiments, respectively. Individual ensemble members are shown with a cross and the ensemble mean with a circle. Columns 4, 5 and 6 show all available members for the CCMI models in three groups: CCMI-REF-C1, CCMI-REF-C2-uncoupled where SSTs and sea ice are prescribed from another climate model, and CCMI-REF-C2-coupled (ACCESS-CCM = red cross, CESM1 CAM4-Chem = blue, CMAM = magenta,

EMAC-L47MA = grey, EMAC-L90MA = dark green, GEOSCCM = purple, MRI-ESM = pale green, NIWA-UKCA = yellow, SOCOL = orange).

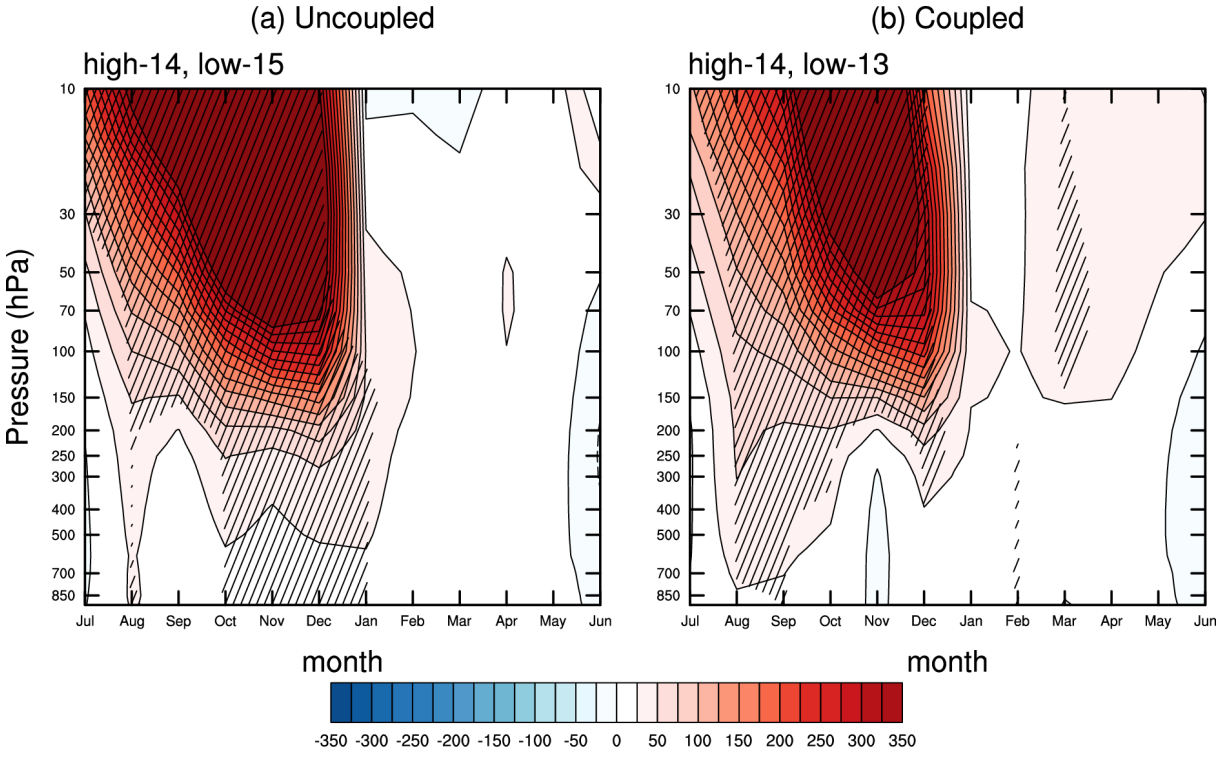

FIG. 6. Time-height evolution of the composite differences (high – low ozone) between the years with the highest and lowest (magnitude exceeds one standard deviation; number of years indicated at the top left of each column) polar cap (63-90°S) averaged November ozone values (1979-2004) for vertically resolved polar cap average geopotential height [m]. Left: composite differences for WACCM uncoupled experiment; right: coupled experiment. Hatching indicates differences that are statistically significant at the 95% level.

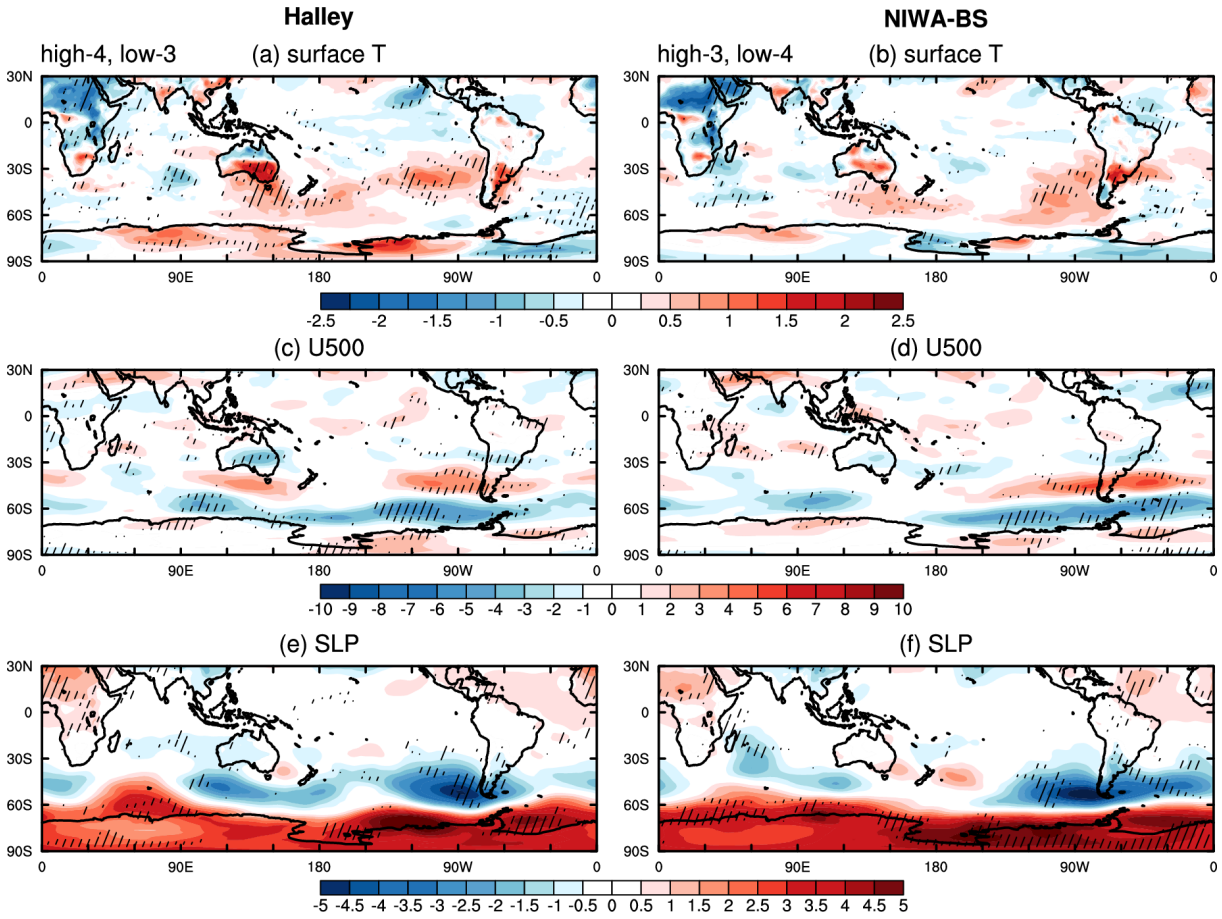

FIG. 7. Composite differences (high – low ozone) in summer between the years with the highest and lowest (magnitude exceeds one standard deviation; number of years indicated at the top left of each column) November ozone values (1979-2004). (a, b) Surface temperature [K]. (c, d) Zonal wind at 500 hPa [m s^{-1}]. (e, f) Sea level pressure (SLP) [hPa]. Left: composite differences for Halley ozone; right: for NIWA-BS ozone. Hatching indicates differences that are statistically significant at the 95% level.

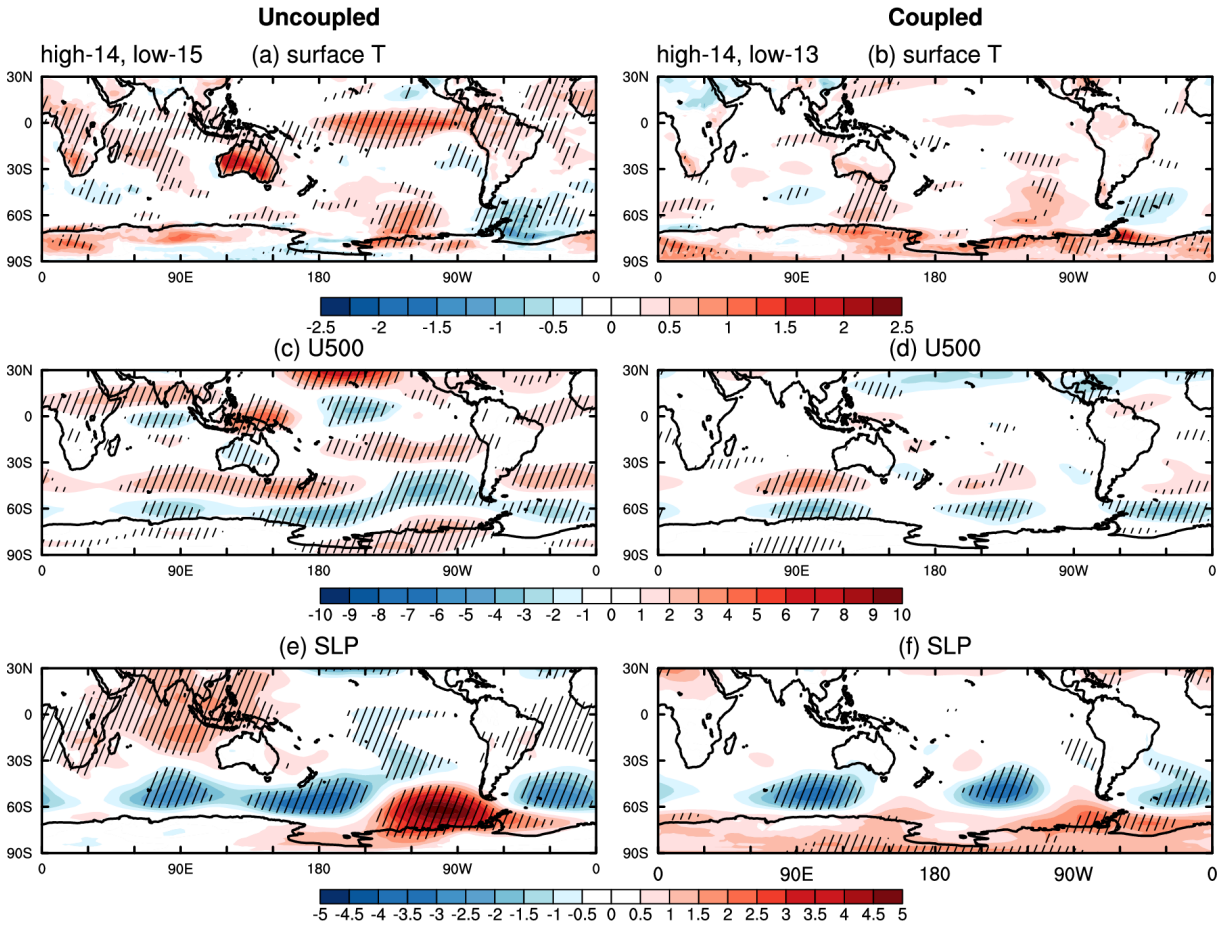

FIG. 8. As in Fig. 7, but for WACCM. Left: composite differences for the uncoupled experiment; right: for coupled experiment.

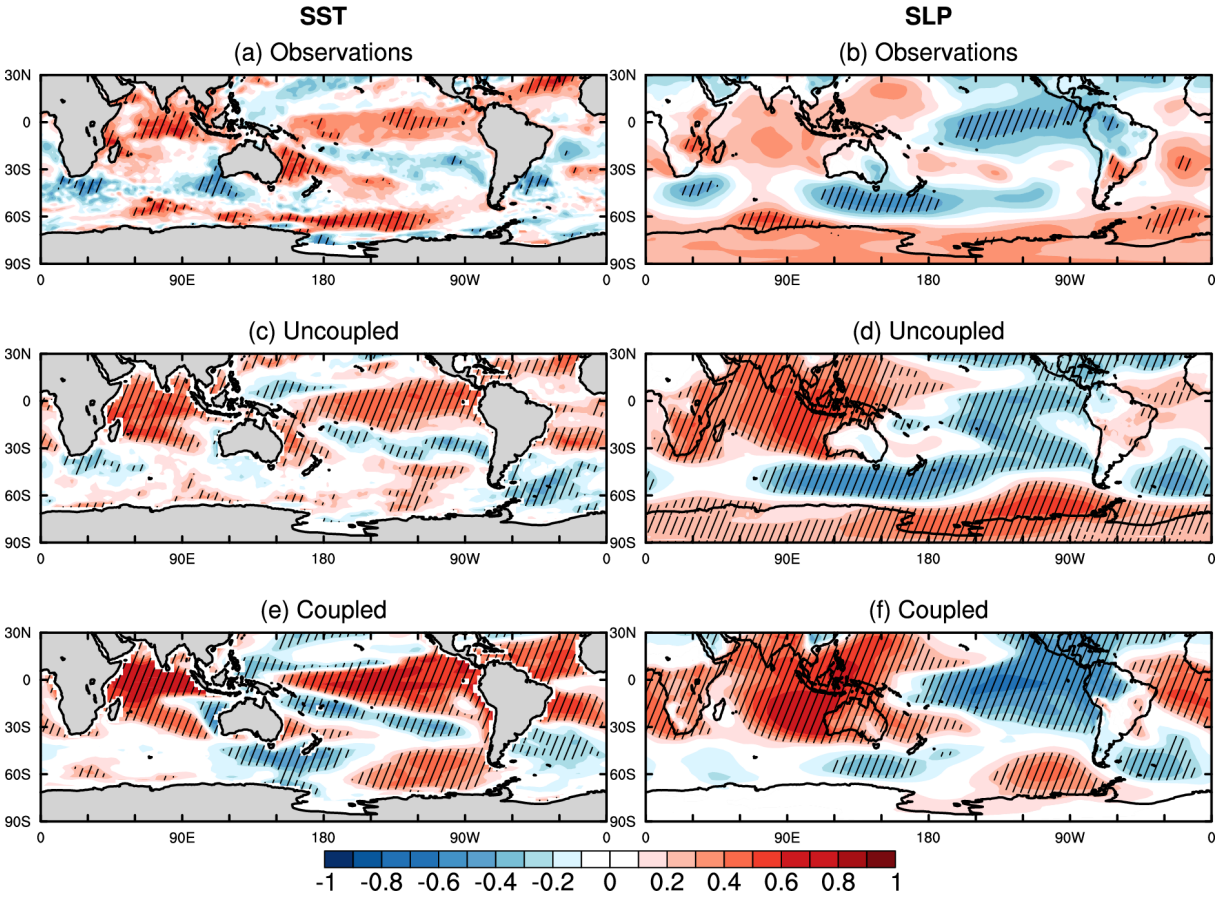

FIG. 9. Correlation coefficients between detrended Eastern Australia summer surface temperatures and detrended summer SSTs and SLP (1979-2004) for (a, b) observations, and (c, d) uncoupled and (e, f) coupled WACCM experiments. Hatching indicates correlations that are statistically significant at the 95% level.

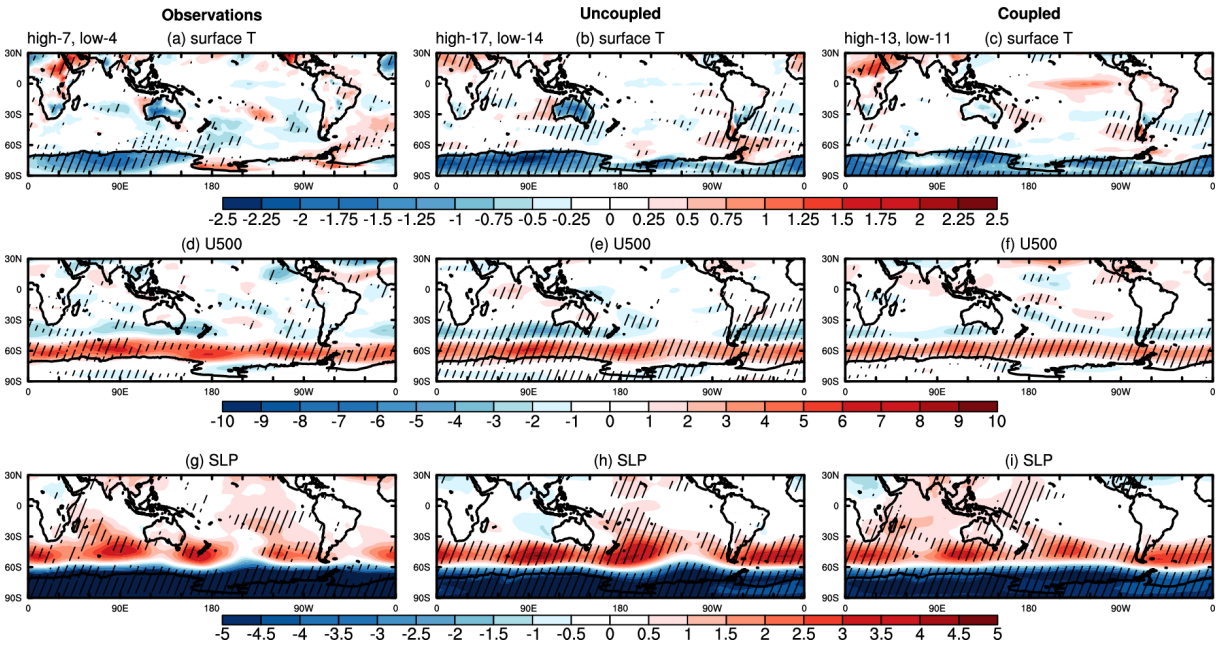

FIG. 10. As in Figs. 7 and 8, but for the composite differences (high – low SAM) in summer between the positive and negative phases of the summer SAM (when the magnitude exceeds one standard deviation; number of years indicated at the top left of each column). (a, d, g) observations, and (b, e, h) WACCM uncoupled and (c, f, i) coupled experiments.